Geol. Mag. **144** (6), 2007, pp. 937–952. © 2007 Cambridge University Press
doi:10.1017/S0016756807003834 First published online 21 August 2007 *Printed in the United Kingdom*

Elemental and Sr–Nd–Pb isotopic geochemistry of Mesozoic mafic intrusions in southern Fujian Province, SE China: implications for lithospheric mantle evolution

JUN-HONG ZHAO*‡, RUIZHONG HU*, MEI-FU ZHOU† &SHEN LIU*

*Institute of Geochemistry, Chinese Academy of Geosciences, Guiyang, Guizhou. China
†Department of Earth Sciences, the University of Hong Kong, Hong Kong

(*Received* 3 October 2006; *accepted* 18 January 2007)

Abstract – Cretaceous mafic dykes in Fujian province, SE China provide an opportunity to examine the nature of their mantle source and the secular evolution of the Mesozoic lithospheric mantle beneath SE China. The mafic rocks have SiO_2 ranging from 47.42 to 55.40 wt %, Al_2O_3 from 14.0 wt % to 20.4 wt %, CaO from 4.09 to 11.7 wt % and total alkaline (K_2O+Na_2O) from 2.15 wt % to 6.59 wt %. Two types are recognized based on their REE and primitive mantle-normalized trace element patterns. Type-A is the dominant Mesozoic mafic rock type in SE China and is characterized by enrichment of light rare earth elements (LREE) ((La/Yb)n = 2.85–19.0) and arc-like trace element geochemistry. Type-P has relatively flat REE patterns ((La/Yb)n = 1.68–3.43) and primitive mantle-like trace element patterns except for enrichment of Rb, Ba and Pb. Type-A samples show EMII signatures on the Sr-Nd isotopic diagram, whereas type-P rocks have high initial $^{143}Nd/^{144}Nd$ ratios (0.5126–0.5128) relative to the type-A rocks ($^{143}Nd/^{144}Nd$ = 0.5124–0.5127). The type-A rocks have $^{207}Pb/^{204}Pb$ ranging from 15.47 to 15.67 and $^{206}Pb/^{204}Pb$ from 18.26 to 18.52. All the type-A rocks show a negative correlation between $^{143}Nd/^{144}Nd$ and $^{206}Pb/^{204}Pb$ ratios and a positive relationship between $^{87}Sr/^{86}Sr$ and $^{206}Pb/^{204}Pb$ ratios, indicating mixing of a depleted mantle source and an EMII component. Geochemical modelling shows that the parental magmas were formed by 5–15 % partial melting of a spinel lherzolite, and contaminated by less than 1 % melt derived from subducted sediment. The type-P magmas were derived from a mantle source unmodified by subduction components. The wide distribution of type-A dykes in SE China suggests that subduction-modified lithospheric mantle was extensive beneath the Cathaysia Block. Geochemical differences between Mesozoic and Cenozoic mafic rocks indicate that lithospheric thinning beneath SE China occurred in two episodes: firstly by heterogeneous modification by subducted components in early Mesozoic times, and later by chemical–mechanical erosion related to convective upwelling of the asthenosphere during Cenozoic times.

Keywords: Mesozoic, mafic dykes, mantle evolution, SE China.

1. Introduction

In North China, the Palaeozoic lithosphere was as much as 200 km thick (Wang *et al.* 2000) and was thinned to 80 km in the Cenozoic as revealed by mantle xenoliths from Cenozoic basalts (Fan *et al.* 2000). Thus, at least 120 km of rigid lithospheric mantle was removed during the Mesozoic (Zhang & Sun, 2002; Zhang *et al.* 2003). Although thinning of the lithospheric mantle from the Palaeozoic to Cenozoic in South China was inferred by Xu *et al.* (2000), the change was poorly documented and the processes involved were unknown because of the paucity of Palaeozoic and Mesozoic mantle-derived rocks. Clearly, the nature of the Mesozoic lithospheric mantle underneath South China is important for understanding mantle evolution in the region and needs to be well documented.

‡Author for correspondence; present address: Department of Earth Sciences, University of Hong Kong, Hong Kong; e-mail: jhzhao@hkusua.hku.hk

Based on spinel peridotite xenoliths in SE China, the Proterozoic subcontinental lithospheric mantle (SCLM) underwent heterogeneous replacement by Phanerozoic mantle before late Jurassic times (Zheng *et al.* 2004). In the Mesozoic, an arc-like mantle was formed by modification of previous material (Li & McCulloch, 1998; Wang, 2002; Zhao, Hu & Liu, 2004; Xie *et al.* 2006), and in the Cenozoic the lithosphere had OIB-like affinities according to basalts in SE China (Chung *et al.* 1994, 1995; Ho *et al.* 2003; Zheng *et al.* 2004). Thus, the Mesozoic mafic intrusions provide a good opportunity to investigate the lithospheric mantle evolution beneath South China. Although mafic dykes in SE China, such as in Jiangxi province (Xie *et al.* 2006) and Guangdong province (Li & McCulloch, 1998), have been previously reported, mafic dykes in Fujian province have not been extensively studied. This paper reports major and trace element compositions and Sr–Nd–Pb isotopic data for selected mafic intrusions in Fujian province, accompanied by previously published data for mafic dykes in Jiangxi

and Guangdong provinces. Our objectives are: (1) to determine the nature of the Mesozoic mantle source for the mafic rocks; (2) to constrain the processes and mechanism(s) related to their formation; and (3) to provide a better understanding of the evolution of the lithospheric mantle beneath SE China.

2. Geological background

South China was formed by amalgamation of the Yangtze Block to the west and the Cathaysia Block to the east along a Neoproterozoic collision belt (Chen & Jahn, 1998). The Yangtze Block is composed of basement complexes overlain by a Neoproterozoic (Sinian) to Cenozoic cover sequence (Zhou *et al.* 2006). The Cathaysian Block collided with the Yangtze Block at about 1000 Ma and consists of Proterozoic basement and Sinian to Triassic sedimentary strata (Chen & Jahn, 1998).

The coastal area of Fujian province in SE China lies within the Cathaysian Block and is adjacent to the Pacific Plate (Fig. 1). Two NE-trending faults, the Changle–Nanao and Zhenhe–Dapu fault, separate the area into three tectonic belts from east to west, the Pingtan–Dongshan metamorphic belt, the Cretaceous magmatic belt and the Early Palaeozoic foldbelt.

The Pingtan–Dongshan metamorphic belt is composed of lower Palaeozoic regionally metamorphosed rocks, late Mesozoic granites, volcanic rocks and mafic–ultramafic rocks. The metamorphic rocks include biotite gneiss, amphibolite, sillimanite schist and quartz schist. These rocks have Rb–Sr isochron ages of 165–178 Ma (Jahn, Chen & Yan, 1976; Lu *et al.* 1994).

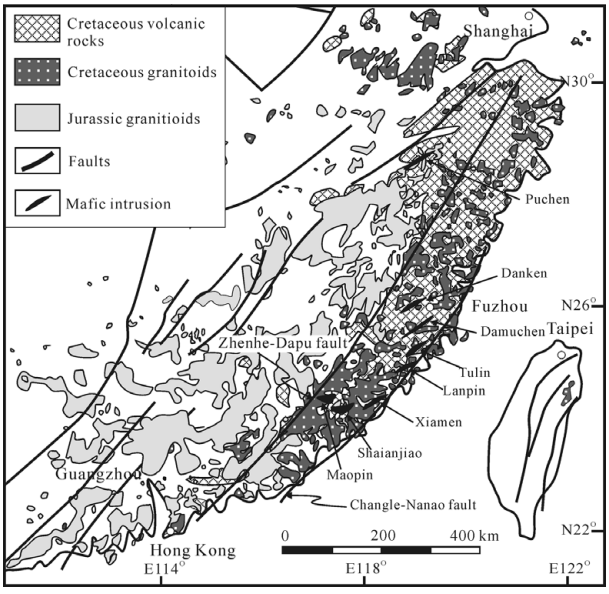

Figure 1. Simplified geological map of SE China showing the distribution of the Late Mesozoic magmatic rocks (modified from Li, 2000) and location of sampled mafic dykes and intrusions.

Mafic–ultramafic rocks occur only along the Changle–Nanao fault, and have been dated at 95–115 Ma using the zircon U–Pb method (Li *et al.* 1995; Dong *et al.* 1997) and whole rock Sm–Nd method (Wang, 2002).

The Cretaceous magmatic belt, which is 500 km long and 100 km wide, is composed of Cretaceous granitic and volcanic rocks (Fig. 1) (Li, 2000). The granitic rocks include Early Cretaceous I-type granites and minor Late Cretaceous A-type granites. Based on Rb–Sr and K–Ar dating results, the I-type granites have ages of 165 Ma and 120–90 Ma (Jahn, Chen & Yan, 1976), whereas the A-type granites have ages of 90 to 70 Ma (GMRBF, 1985). The plutonic rocks intruded upper Triassic to upper Jurassic sandstone, volcanic rocks and phyllite and form a distinct calc-alkaline magmatic belt.

The Early Palaeozoic fold belt to the west consists of a Proterozoic basement known as the Mayuan and Mamianshan complexes (Jin & Sun, 1997), overlain by Cambrian and Triassic strata. Granites are widely distributed in this belt, and have variable ages ranging from 120 Ma to 500 Ma (Li, 2000).

Relatively abundant mafic intrusions in the Cretaceous magmatic belt include mafic plutons, such as the Maopin and Shaianjiao bodies, and numerous mafic dykes (Fig. 1). Both of the plutons are sill-like bodies, about 3 km long and 1.5 km wide, and are composed of relatively undifferentiated mafic rocks. They intrude Jurassic tuffs and Triassic strata and the Tianling muscovite granite which has been dated at 138 Ma by the K–Ar method (GMRBF, 1985). Locally, the intrusions have chilled margins against their hosts. Mafic dykes, which also intrude the Mesozoic successions, are typically several metres wide and mostly trend NE. These dykes, which crop out in the coastal area of Fujian province, include the Damuchen, Danken, Xiamen, Tulin, Lanpin and Puchen bodies that were investigated in this study (Fig. 1). Rocks from both the mafic plutons and dykes are massive and are composed mainly of clinopyroxene and plagioclase with minor Fe–Ti oxides and quartz.

3. Analytical methods

Relatively fresh samples were collected with care to avoid weathered, hydrothermally altered and mineralized parts. Whole-rock samples were trimmed to remove slightly weathered surfaces, and then powdered using an agate mill. K–Ar age determinations were carried out utilizing the MM1200 spectrometer at the Institute of Geology, China Seismology Bureau. Parameters used were: $\lambda_e = 0.581\times10^{-10}$ year^{-1}, $\lambda_\beta = 4.962\times10^{-10}$ year^{-1}; ^{40}K = 0.01167 atom % (Steiger & Jäger, 1977).

The major oxides were analysed by routine wet chemistry with precisions better than ± 2 %. Trace elements, including REE, were analysed using a Finnigan Element ICP-MS at the Institute of Geochemistry,

https://doi.org/10.1017/S0016756807003834 Published online by Cambridge University Press

Chinese Academy of Sciences (CAS), following the procedures described in Qi, Hu & Gregoire (2000). Precisions are within ± 5–10 %.

Sr and Nd isotopic compositions were determined using a Micromass Isoprobe MC-ICPMS at the Guangzhou Institute of Geochemistry. $^{87}Sr/^{86}Sr$ ratios of the NBS 987 and $^{143}Nd/^{144}Nd$ ratios of Shin Etsu JNDi-1 standard measured during this study were 0.710243 ± 14 (2σ) and 0.512124 ± 11 (2σ), respectively. Detailed descriptions of the analytical techniques can be found in Li *et al.* (2004).

For Pb-isotope determination, 200 mg of sample powder were placed into a Teflon® beaker, spiked and dissolved in concentrated HF at 800 °C for 72 hours. Pb was separated and purified by conventional ion-exchange techniques with 0.5 M HBr as eluant followed by 2 M HCl leaching and collection of the Pb in 1.5 ml of 6 M HCl. Samples were then dried on a hot plate under a lamp in a nitrogen gas flow tank for about two hours. Isotope ratios were measured at the Isotope Analysis Center of the Institute of Geology, Beijing Nucleus Industry, using a MAT261 thermal ionization mass spectrometer. During the course of this study, measured ratios of the NBS981 Pb standard were $^{208}Pb/^{206}Pb = 2.165246 \pm 69$, $^{207}Pb/^{206}Pb = 0.914510 \pm 56$ and $^{204}Pb/^{206}Pb = 0.059199 \pm 13$.

4. Analytical results

Whole-rock samples have K–Ar ages ranging from 108 to 130 Ma (Table 1). These ages are in agreement with the field relationships.

Samples from the Danken, Tulin and Lanpin dykes have loss on ignition (LOI) up to 6 wt %, whereas those from the Shaianjiao and Maopin intrusions have LOI less than 3 wt %, indicating weak to moderate alteration. High field strength (HFSE) and rare earth elements (REE) are essentially immobile under such conditions (e.g. Pearce & Cann, 1973; Whalen, Syme & Stern, 1999), thus we focus mainly on these elements to constrain the petrogenesis of the rocks.

4.a. Major and trace elements

Forty-eight representative samples from the two mafic plutons and six mafic dykes were analysed (Table 2).

Table 1. K–Ar ages for rocks from the Maopin and Shaianjiao intrusions, Fujian Province, SE China

Sample	K (wt %)	^{40}Ar (mol/g)	$^{40}Ar_a$ (%)	Apparent age (Ma) ± 1σ
Maopin intrusion				
SY-20	0.40	7.722E-10	64.96	108.0 ± 3.6
Shaianjiao intrusion				
XC-4	1.11	2.598E-10	82.85	130.2 ± 3.2
XC-5	0.21	4.742E-11	53.83	125.7 ± 5.4

Parameters for ^{40}K: $\lambda_e = 0.581 \times 10^{-10}$ year^{-1}, $\lambda_\beta = 4.962 \times 10^{-10}$ year^{-1}; $^{40}K = 0.01167$ atom % (Steiger & Jäger, 1977).

Both the plutons and dykes have similar chemical compositions and are tholeiitic in terms of a SiO_2 v. (K_2O+Na_2O) plot (Fig. 2). SiO_2 ranges from 47.42 to 55.40 wt %, MgO from 3.05 to 6.76 wt %, Fe_2O_3 from 1.91 to 6.51 wt % and CaO from 4.09 to 11.68 wt % (Table 2). SiO_2 correlates negatively with MgO and CaO. The Al_2O_3 contents of the rocks vary from 14.02 to 20.39 wt % and K_2O+Na_2O from 2.15 to 6.59 wt % (Table 2).

The intrusions are divided into two types, type A and type P, based on their geochemistry. Type-A rocks are slightly enriched in LREE, with $(La/Yb)_n$ ratios ranging from 2.85 to 19.0 (Fig. 3a), and have arc-like primitive mantle-normalized patterns with enrichment of large ion lithophile elements (LILE: Rb, Ba, Th and U), depletion of high field strength elements (HFSE: Nb, Ta, Zr and Hf) and positive Pb and negative Ti anomalies (Fig. 4a). Type-P rocks are characterized by flat REE patterns with (La/Yb)n ratios of 1.68 to 3.43 (Fig. 3b) and flat primitive mantle-normalized trace element patterns with slight enrichment of Rb, Ba and Pb (Fig. 4b). Both types of mafic rocks have low Nb/U (1.70–27.13), Ce/Pb (0.49–7.40) and La/Th (< 16.57) ratios except for those from the Danken body, which have high Nb/U (41.17–46.72) and Ce/Pb (6.32–9.44) ratios, compared with primitive mantle and N-MORB values (Sun & McDonough, 1989).

4.b. Sr–Nd and Pb–Pb isotopes

Age-corrected $^{87}Sr/^{86}Sr$ ratios for the type-A samples range from 0.7047 to 0.7078 (Table 3), and the high $^{87}Sr/^{86}Sr$ and low $^{143}Nd/^{144}Nd$ (0.5124–0.5129) ratios form a trend roughly toward enriched mantle type II (EMII) (Fig. 5). The type-P samples from the Puchen and Danken dykes have slightly higher average $^{143}Nd/^{144}Nd$ (0.5127–0.5129) and $^{87}Sr/^{86}Sr$ ratios (0.7068–0.7073) except for sample DC6. All the samples from Fujain province have $^{87}Sr/^{86}Sr$ and $^{143}Nd/^{144}Nd$ ratios similar to those of the late Mesozoic mafic dykes in Jiangxi and Guangdong provinces (Li & McCulloch, 1998; Xie *et al.* 2006). Rocks from the Maopin and Shaianjiao intrusions have a narrow range of $^{206}Pb/^{204}Pb$ (18.26–18.52) with slightly more radiogenic ^{207}Pb and ^{208}Pb than ^{206}Pb (Fig. 6). Their $^{208}Pb/^{204}Pb$ and $^{207}Pb/^{204}Pb$ ratios range from 38.2 to 38.8 and from 15.5 to 15.7, respectively (Table 3).

5. Discussion

5.a. Effects of crustal contamination

Crustal contamination commonly plays an important role during magma emplacement and its effects must be evaluated carefully. Samples from the Lanpin, Xiamen and Damuchen dykes show negative correlations between Y and Zr/Y ratios, suggesting a significant addition of crustal components to their primary

https://doi.org/10.1017/S0016756807003834 Published online by Cambridge University Press

Table 2. Major oxides and trace element compositions for mafic rocks from Fujian province, SE China

Location	Damuchen dyke						Lanpin dyke				Tuin dyke						Xyamen dyke						Maopin pluton	
Sample	DMC1	DMC4	DMC5	DMC7	DMC8	DMC13	LP1	LP3	LP5	LP6	TL1	TL3	TL5	TL7	TL8	TL10	XM1	XM3	XM4	XM6	XM7	XM8	SY13	SY14
Major elements (wt %)																								
SiO_2	55.40	53.52	52.41	49.20	54.95	52.19	49.47	51.11	53.93	54.42	50.91	53.03	51.26	54.77	50.06	51.18	50.06	52.25	52.37	53.03	50.10	52.77	47.42	52.68
TiO_2	1.60	1.75	1.72	1.63	1.66	1.91	1.85	1.91	1.35	1.38	1.54	0.92	1.41	0.98	1.23	1.88	1.69	1.54	1.63	1.48	1.69	1.54	0.75	0.75
Al_2O_3	17.18	17.39	18.02	20.08	17.40	17.10	18.63	17.01	17.18	17.71	18.24	16.79	17.78	16.25	17.32	17.24	20.08	20.39	19.24	18.63	20.12	19.47	14.02	14.78
Fe_2O_3	5.08	3.62	3.01	3.75	2.32	3.12	3.30	3.19	2.09	2.73	3.41	1.98	2.93	2.19	3.15	3.19	3.74	3.70	3.88	3.07	3.46	3.50	2.68	2.68
FeO	3.10	5.10	5.25	4.05	5.60	5.15	4.90	5.10	3.90	3.10	4.93	3.70	4.40	3.55	4.25	4.95	3.67	3.80	3.67	3.20	3.10	3.57	7.72	6.85
Fe_2O_3T	8.52	9.29	8.84	8.25	8.54	8.84	8.74	8.86	6.42	6.17	8.89	6.09	7.82	6.13	7.87	8.69	7.82	7.92	7.96	6.63	6.90	7.47	11.26	10.29
MnO	0.27	0.25	0.27	0.24	0.26	0.21	0.23	0.26	0.21	0.20	0.22	0.20	0.23	0.22	0.26	0.24	0.20	0.20	0.24	0.24	0.23	0.21	0.24	0.18
MgO	3.40	3.48	3.71	4.10	3.05	3.74	4.85	4.48	5.43	5.57	4.45	5.67	4.92	5.76	6.16	4.00	3.49	3.60	3.91	4.57	3.11	3.44	6.27	5.89
CaO	6.00	6.99	7.13	8.01	6.12	6.22	7.46	7.01	4.39	4.09	6.10	7.59	6.88	8.02	9.61	8.03	7.07	6.03	7.01	6.10	7.92	6.71	9.90	10.84
Na_2O	3.78	3.71	3.78	3.39	3.64	3.91	4.30	4.34	3.62	3.52	4.10	1.84	3.76	2.44	1.97	3.14	3.17	4.21	4.09	3.14	3.86	3.84	1.95	2.32
K_2O	1.72	1.72	1.81	1.40	1.80	1.85	1.33	1.24	2.97	2.80	0.97	1.11	0.88	0.79	0.42	0.96	1.33	1.00	1.00	1.81	1.49	1.30	0.20	0.16
P_2O_5	0.20	0.16	0.30	0.10	0.20	0.27	0.37	0.33	0.32	0.40	0.40	0.08	0.40	0.17	0.10	0.40	0.27	0.28	0.27	0.42	0.40	0.37	0.50	0.43
LOI	2.12	1.50	2.00	3.30	2.15	3.50	2.70	3.10	3.98	4.01	4.01	6.20	4.38	4.05	4.70	4.10	4.53	2.10	2.00	3.60	3.50	2.80	6.39	1.50
Total	100	99.59	99.87	99.85	99.65	99.62	99.79	99.43	99.37	99.93	99.58	99.67	99.69	99.79	99.86	99.86	99.7	99.4	99.78	99.89	99.48	99.92	99.34	99.36
Trace elements (ppm)																								
Ba	544	534	474	360	530	562	1320	793	1548	1385	483	576	677	424	512	1160	1390	743	734	941	776	2280	111	100
Rb	83.9	78.0	73.5	46.2	87.6	94.8	55.8	39.7	147.6	131.6	30.5	37.1	38.1	34.6	18.1	45.7	36.9	29.2	27.4	50.3	34.6	38.2	35.7	16.5
Sr	364	347	325	404	355	363	839	492	826	801	402	436	603	393	345	1112	724	673	700	575	660	771	363	384
Y	25.3	28.7	24.4	20.8	25.9	28.0	22.4	21.6	22.2	21.8	18.0	15.0	33.3	15.3	14.9	24.1	31.5	29.0	30.4	24.7	24.1	39.1	33.7	34.0
Zr	148	142	137	105	150	153	111	111	135	136	101	67	100	68	71	137	140	147	143	226	140	149	140	150
Nb	8.51	7.95	7.54	5.51	8.67	8.35	6.38	6.82	6.22	6.18	6.01	4.36	5.35	4.41	2.80	8.00	6.74	7.07	6.81	12.48	6.74	6.95	12.93	13.10
Th	8.57	7.99	7.65	4.75	8.99	8.26	2.49	2.61	8.91	8.74	2.49	3.69	2.61	3.72	1.26	2.15	2.02	2.00	1.93	3.49	1.96	2.05	2.09	2.00
Ni	51.9	58.8	60.8	91.5	46.7	70.1	45.8	49.8	104.1	123.8	67.1	116.8	94.9	121.4	155.2	47.9	49.3	48.9	44.4	108.9	45.0	65.5	104.3	123.4
V	203	208	206	200	195	222	216	212	164	171	189	158	189	156	202	209	189	201	192	156	186	199	281	303
Cr	31.7	36.7	29.4	45.9	23.6	51.4	63.2	59.0	187.9	229.8	90.7	381.5	198.2	385.5	492.4	58.4	35.8	43.7	41.8	168.9	42.9	43.5	192.1	177.1
Hf	4.68	4.47	4.08	3.22	4.77	4.35	3.38	3.35	3.99	4.07	3.02	2.31	2.94	2.26	2.22	3.76	4.13	4.24	4.04	5.94	3.97	4.25	4.25	4.21
Sc	21.5	21.2	21.3	23.0	20.8	23.9	22.3	22.2	17.1	17.6	18.8	18.7	19.3	19.0	23.2	21.0	18.4	20.2	18.4	18.5	17.0	18.7	32.8	32.3
Ta	0.51	0.48	0.44	0.32	0.56	0.49	0.38	0.40	0.33	0.30	0.35	0.36	0.31	0.37	0.15	0.44	0.35	0.36	0.35	0.55	0.34	0.36	0.75	0.81
U	1.65	1.51	1.47	0.88	1.70	1.45	0.56	0.70	3.66	2.36	0.69	1.61	0.90	1.55	0.30	0.56	0.46	0.53	0.46	0.79	0.44	0.59	0.56	0.55
W	1.55	1.65	1.59	1.51	1.48	1.66	1.71	1.60	2.13	2.02	1.77	1.22	1.46	1.26	1.22	1.67	1.81	1.51	1.72	1.52	1.64	1.78	1.66	1.73
Pb	9.14	9.87	9.75	6.65	9.98	12.82	8.47	18.64	22.29	25.56	7.28	9.98	8.43	13.47	7.85	13.53	10.96	8.55	10.93	23.45	9.94	11.86	74.10	51.60
P	873	698	1309	436	873	1178	1615	1440	1397	1746	1746	349	1746	742	436	1746	1178	1222	1178	1833	1746	1615	2182	1877
La	28.6	29.0	26.0	18.3	28.9	32.1	17.8	18.8	47.7	46.8	20.0	12.4	22.3	11.7	10.2	24.7	28.1	33.1	32.5	35.6	24.3	30.4	14.9	15.2
Ce	58.0	56.5	53.1	37.4	59.1	66.2	39.9	40.6	102.5	101.7	42.6	26.9	39.6	25.9	23.1	54.1	52.8	63.3	59.4	74.2	51.7	54.4	36.5	37.1
Pr	6.60	6.69	6.21	4.44	6.88	7.09	5.20	5.14	12.70	12.76	5.32	3.18	5.90	3.23	3.16	6.84	7.11	8.86	8.21	8.67	6.41	7.77	4.76	4.98
Nd	26.8	26.3	25.0	18.4	28.0	28.5	23.2	23.1	54.7	54.3	24.0	13.5	26.4	14.2	13.1	31.2	30.8	37.4	34.8	35.0	28.0	34.1	22.8	22.8
Sm	5.39	5.58	5.39	3.88	5.78	5.86	5.20	4.95	10.07	9.76	4.92	3.05	5.89	3.08	3.13	5.85	6.16	7.52	6.95	6.63	5.58	6.87	5.63	6.01
Eu	1.46	1.52	1.44	1.33	1.51	1.71	1.77	1.75	2.46	2.41	1.52	0.84	1.74	0.90	0.96	1.97	1.76	2.16	2.00	1.74	1.67	1.83	1.98	2.25
Gd	5.20	5.36	4.97	4.18	5.49	5.58	5.03	4.86	7.02	6.60	4.21	2.62	5.76	2.75	2.73	5.57	5.67	6.43	6.29	5.55	5.09	6.48	5.93	6.31
Tb	0.77	0.84	0.77	0.65	0.81	0.88	0.74	0.68	0.84	0.82	0.62	0.43	0.85	0.45	0.43	0.74	0.90	0.94	0.91	0.79	0.71	1.00	1.06	1.13
Dy	4.59	4.97	4.33	3.93	4.62	5.01	4.18	4.09	4.13	4.01	3.34	2.54	5.02	2.48	2.51	4.22	4.70	5.58	4.99	4.16	3.77	5.43	5.99	6.66
Ho	0.90	1.04	0.85	0.78	0.93	0.99	0.79	0.76	0.75	0.76	0.66	0.54	1.03	0.52	0.53	0.81	0.92	1.10	1.04	0.86	0.78	1.10	1.15	1.23
Er	2.58	2.70	2.30	2.02	2.51	2.74	2.24	2.17	2.02	1.91	1.67	1.49	2.75	1.50	1.50	2.21	2.48	2.88	2.59	2.38	2.07	3.05	3.18	3.46
Tm	0.35	0.36	0.32	0.29	0.36	0.36	0.29	0.29	0.27	0.25	0.24	0.23	0.38	0.23	0.21	0.32	0.35	0.44	0.37	0.32	0.30	0.39	0.41	0.48
Yb	2.27	2.33	2.19	1.95	2.50	2.43	1.97	1.95	1.80	1.84	1.60	1.60	2.67	1.62	1.59	2.02	2.24	2.84	2.42	2.36	1.97	2.57	2.90	2.96
Lu	0.35	0.34	0.29	0.27	0.33	0.37	0.28	0.26	0.28	0.26	0.21	0.23	0.37	0.23	0.22	0.29	0.31	0.38	0.35	0.33	0.28	0.41	0.40	0.41

Table 2. Continued.

Location	Maopin pluton			Shaianjiao pluton									Danken dyke						Puchen dyke					
Sample	SY18	SY19	SY20	XC1	XC2	XC3	XC4	XC5	XC6	XC7	XC8	XC9	DC1	DC3	DC5	DC6	DC9	DC11	PC1	PC3	PC4	PC5	PC6	PC7
Major elements (wt %)																								
SiO_2	49.92	52.79	48.06	49.00	49.58	52.85	49.63	51.70	52.73	49.56	51.43	48.59	50.89	49.31	50.56	49.16	48.90	50.27	49.00	49.20	49.07	49.37	49.62	48.10
TiO_2	1.12	0.65	0.60	0.70	0.52	1.10	0.65	0.65	0.50	0.82	0.92	0.62	2.66	2.46	2.65	2.66	2.28	2.03	1.63	1.60	2.15	1.78	1.66	1.91
Al_2O_3	16.84	16.62	19.90	17.71	17.06	14.43	14.56	16.40	15.53	15.31	15.74	16.87	14.03	15.04	15.05	16.10	15.15	16.18	16.17	17.55	16.71	17.39	16.79	17.40
Fe_2O_3	2.60	2.60	3.00	3.62	3.09	1.91	2.63	3.43	1.96	2.44	2.35	3.23	6.51	6.14	5.08	5.08	6.14	5.32	3.71	3.16	2.57	2.50	4.10	3.45
FeO	7.36	6.90	7.10	6.30	6.75	7.60	7.77	6.90	5.90	6.92	7.90	7.90	6.10	6.10	5.95	6.10	6.20	6.13	6.70	6.10	7.31	7.05	7.10	6.90
Fe_2O_3T	10.78	10.27	10.89	10.62	10.59	10.35	11.26	11.10	8.51	10.13	11.13	12.01	13.29	12.92	11.69	11.86	13.03	12.13	11.15	9.94	10.69	10.33	11.99	11.12
MnO	0.22	0.24	0.27	0.30	0.29	0.30	0.31	0.22	0.23	0.29	0.25	0.28	0.29	0.30	0.26	0.30	0.31	0.27	0.29	0.34	0.35	0.34	0.27	0.28
MgO	4.87	4.52	4.58	5.94	5.78	6.20	6.25	5.43	5.97	6.76	5.43	4.94	4.06	4.62	4.71	4.69	4.58	4.66	5.84	5.28	6.05	6.07	6.07	6.00
CaO	10.78	9.76	9.68	10.01	10.40	9.55	10.44	9.60	9.51	11.21	9.71	10.95	6.28	7.22	7.16	7.30	9.62	7.86	10.12	10.63	11.26	11.68	10.27	10.51
Na_2O	2.97	2.74	2.53	1.89	1.62	2.25	2.29	2.28	2.08	1.98	2.30	1.93	3.55	3.63	3.58	3.43	3.57	3.81	2.71	2.59	2.57	2.54	2.41	2.49
K_2O	0.28	0.53	0.48	0.34	0.72	0.96	1.61	0.25	1.34	0.59	0.23	0.42	0.59	0.56	0.55	0.49	0.01	0.54	0.27	0.27	0.01	0.01	0.22	0.20
P_2O_5	0.46	0.43	0.33	0.23	0.44	0.32	0.33	0.47	0.30	0.23	0.30	0.36	0.25	0.32	0.21	0.22	0.23	0.32	0.06	0.07	0.15	0.03	0.06	0.12
LOI	1.43	1.15	2.05	2.10	1.80	1.65	2.30	1.40	2.50	1.90	1.80	2.25	4.20	3.80	3.80	3.90	3.50	1.50	2.05	2.00	0.86	0.33	0.80	1.70
Total	99.3	99.33	99.83	99.49	99.35	99.47	99.32	99.48	99.25	99.26	99.46	99.34	99.81	99.87	99.86	99.93	99.79	99.34	99.65	99.74	99.76	99.59	99.83	99.81
Trace elements (ppm)																								
Ba	80	152	112	138	107	215	209	131	216	150	116	154	331	366	317	241	267	254	275	198	305	252	178	201
Rb	19.5	40.9	37.4	23.5	79.5	123.8	123.7	14.2	181.2	42.1	12.1	35.8	23.9	27.5	20.9	15.1	10.9	20.7	5.5	21.5	5.9	16.6	24.8	16.6
Sr	370	431	406	379	351	462	450	339	525	344	361	356	362	408	349	344	342	417	271	229	274	248	199	201
Y	39.3	41.9	38.1	32.3	33.0	34.3	34.3	34.7	25.2	31.0	33.0	39.1	44.8	32.1	36.3	31.4	33.6	32.6	26.4	24.5	26.2	24.6	32.0	26.6
Zr	187	202	180	131	134	162	162	148	119	125	140	188	138	131	124	123	123	129	86	74	80	75	80	81
Nb	15.57	16.82	15.47	12.03	12.10	13.95	14.29	13.09	7.75	9.97	12.39	15.91	9.94	9.49	9.39	8.85	9.55	9.04	6.74	6.00	6.20	5.80	6.16	6.20
Th	2.69	4.20	2.51	2.02	1.54	3.14	2.98	2.12	5.34	1.30	2.12	3.53	1.00	1.00	1.00	0.98	0.96	0.97	1.04	0.89	0.92	1.09	0.94	0.97
Ni	51.8	53.4	50.8	50.7	80.7	93.8	97.6	42.5	73.1	131.7	53.2	70.3	94.4	100.9	107.7	100.8	105.1	103.2	62.2	84.9	74.5	84.7	79.7	70.7
V	312	292	303	305	308	293	293	320	219	299	337	329	247	254	238	250	250	244	349	333	347	322	350	350
Cr	245.8	107.6	99.4	186.3	220.4	248.8	254.0	137.3	405.9	363.6	154.7	216.6	67.3	74.8	82.8	78.9	81.2	79.0	153.7	251.1	201.2	249.2	201.7	188.0
Hf	5.18	5.48	4.86	3.70	3.75	4.45	4.57	4.19	3.29	3.73	4.05	5.43	4.25	4.17	4.07	4.06	4.07	3.88	2.77	2.46	2.50	2.38	2.62	2.57
Sc	34.9	35.0	33.2	39.7	40.6	36.4	36.7	39.0	30.4	38.8	41.8	40.1	25.7	25.7	24.5	24.8	26.0	25.8	41.2	42.3	43.1	42.1	43.4	42.8
Ta	0.95	1.04	0.92	0.72	0.74	0.85	0.85	0.83	0.44	0.59	0.76	1.02	0.60	0.54	0.53	0.55	0.55	0.51	0.41	0.37	0.39	0.35	0.42	0.40
U	0.67	1.11	0.65	0.57	0.47	0.76	0.72	0.63	1.49	0.38	0.66	0.82	0.23	0.22	0.20	0.22	0.21	0.21	0.27	0.24	0.23	0.24	0.28	0.24
W	1.61	1.60	1.92	1.65	1.59	1.77	1.79	1.72	1.49	1.60	1.62	1.61	1.58	1.64	1.55	1.63	1.60	1.54	1.17	1.10	1.16	1.21	1.25	1.17
Pb	47.76	12.31	11.27	34.10	17.70	31.97	25.39	15.36	30.36	7.00	55.69	11.61	3.50	3.75	3.21	3.64	4.59	3.55	10.06	9.83	15.81	17.95	14.51	11.19
P	2008	1877	1440	1004	1920	1397	1440	2051	1309	1004	1309	1571	1091	1397	917	960	1004	1397	262	306	655	131	262	524
La	18.6	21.9	17.5	13.5	12.6	18.5	17.3	14.8	26.2	11.0	13.9	20.5	14.8	13.2	13.9	12.9	13.0	13.0	7.3	6.3	6.7	6.5	7.0	7.0
Ce	43.7	50.5	43.0	31.8	31.2	43.5	41.3	35.5	54.4	28.2	33.8	48.4	32.0	29.4	30.3	28.6	29.1	29.1	17.5	15.1	16.2	15.2	16.6	16.8
Pr	5.81	6.54	5.55	4.25	4.24	5.51	5.25	4.56	6.38	3.98	4.37	6.21	4.38	3.88	4.12	3.89	3.77	3.97	2.33	2.07	2.30	2.42	2.32	2.34
Nd	26.6	29.9	26.0	20.5	19.8	24.5	24.6	21.5	26.4	18.8	20.0	28.0	20.8	18.7	19.9	18.3	18.8	17.6	11.7	10.2	11.1	10.9	11.6	11.6
Sm	6.24	7.51	6.79	4.94	4.92	5.67	6.04	4.87	5.12	4.84	4.99	6.78	5.96	5.67	5.74	5.27	5.52	5.32	3.49	3.12	3.16	3.37	3.27	3.61
Eu	2.13	2.30	2.22	1.77	1.91	2.16	2.14	2.03	1.49	1.73	1.94	2.29	2.14	1.93	1.96	1.81	1.94	1.83	1.22	1.19	1.23	1.18	1.35	1.28
Gd	6.56	7.39	6.79	5.28	5.44	6.29	6.09	5.98	4.75	5.50	5.82	7.14	7.27	6.11	6.24	5.88	5.96	6.18	4.07	3.85	3.93	4.01	4.30	4.15
Tb	1.25	1.31	1.24	1.01	0.99	1.11	1.14	1.08	0.76	0.98	1.00	1.24	1.24	1.00	1.06	0.98	1.03	1.01	0.72	0.64	0.68	0.67	0.82	0.68
Dy	7.06	7.64	6.88	5.77	5.70	5.94	6.04	6.19	4.75	5.52	6.02	7.10	7.36	6.00	6.86	5.81	5.97	6.04	4.57	4.49	4.69	4.45	5.03	4.60
Ho	1.40	1.51	1.34	1.06	1.17	1.21	1.22	1.19	0.82	1.15	1.19	1.45	1.52	1.13	1.32	1.16	1.19	1.22	1.00	0.85	0.97	0.93	1.08	0.99
Er	3.93	4.20	3.54	3.04	3.18	3.19	3.24	3.15	2.38	2.89	3.20	3.78	3.68	3.00	3.44	2.89	3.28	3.14	2.89	2.56	2.67	2.52	3.20	2.70
Tm	0.54	0.59	0.51	0.42	0.44	0.45	0.50	0.44	0.35	0.44	0.48	0.51	0.56	0.41	0.50	0.44	0.43	0.43	0.41	0.37	0.42	0.37	0.42	0.39
Yb	3.52	3.71	2.94	2.79	2.84	2.85	2.89	2.86	2.33	2.78	2.82	3.52	3.56	2.77	3.11	2.73	2.92	2.99	2.81	2.64	2.68	2.52	2.98	2.65
Lu	0.50	0.54	0.46	0.37	0.41	0.40	0.46	0.39	0.32	0.39	0.39	0.46	0.57	0.38	0.47	0.40	0.39	0.39	0.39	0.38	0.39	0.35	0.43	0.37

LOI – loss on ignition.

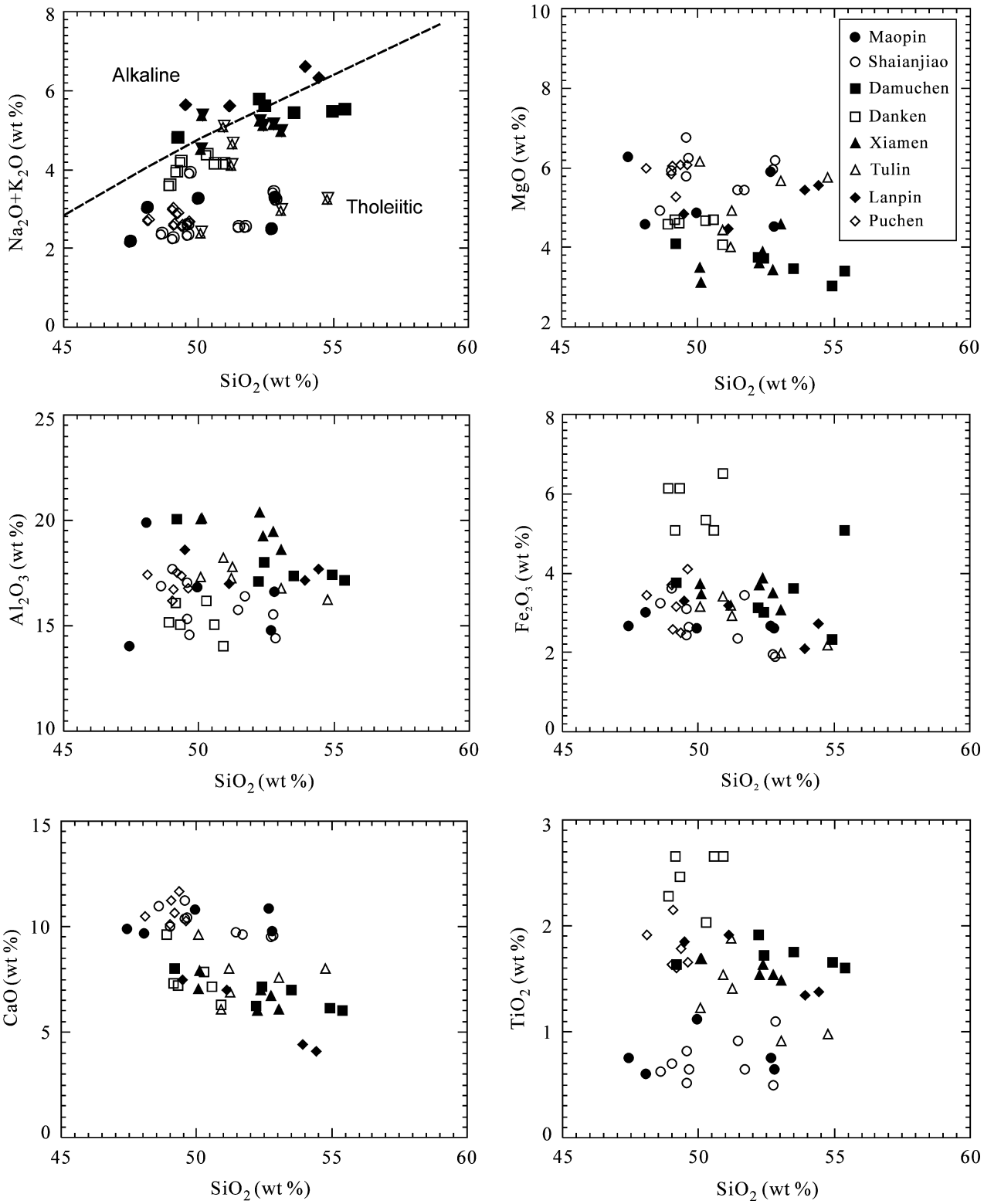

Figure 2. SiO_2 v. other major oxides of the mafic intrusions from the coastal area of the Fujian Province, SE China.

magmas (Fig. 7a). This conclusion is supported by their large variation of εNd (−3.7 to +3.3). Samples from the Damuchen dyke have $^{87}Sr/^{86}Sr$ ratios slightly higher than the average value for Pacific sediments (0.7074) (Plank & Langmuir, 1998) (Fig. 5), further suggesting significant crustal contamination during magma emplacement. Samples from the Maopin and Shaianjiao intrusions have well-defined positive correlations between Y and Zr/Y ratios, suggesting little or no crustal contamination. A lack of crustal contamination in these two intrusions is consistent with their higher Nb and Yb concentrations relative to the

https://doi.org/10.1017/S0016756807003834 Published online by Cambridge University Press

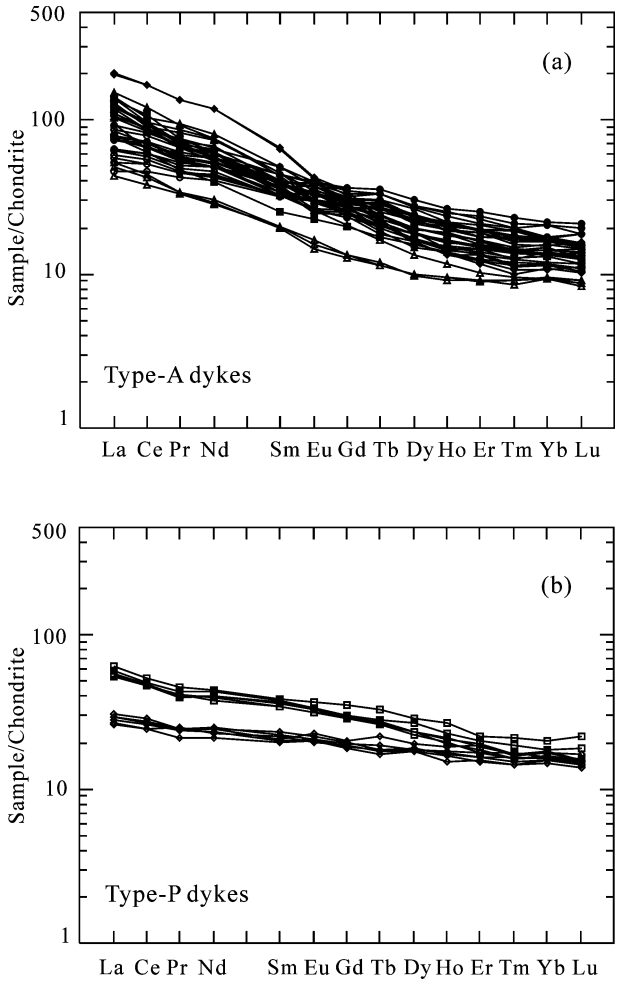

Figure 3. Chondrite-normalized REE patterns for the mafic rocks from the coastal area of the Fujian province, SE China. Type A comprises the Maopin, Shaianjiao, Damuchen, Xiamen, Tulin and Lanpin intrusions which have relatively steeper REE patterns (a) compared with the type-P samples from the Danken and Puchen dykes (b). Normalization values are from Sun & McDonough (1998).

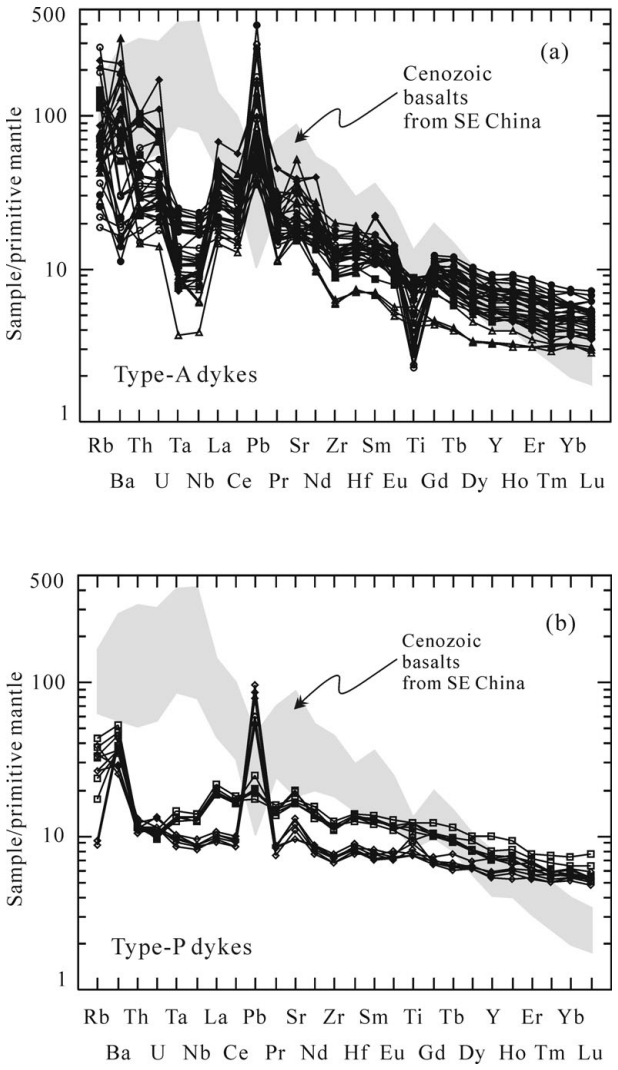

Figure 4. Primitive mantle-normalized trace element diagrams for (a) the type-A and (b) type-P mafic rocks from the coastal area of Fujian province, SE China. Primitive mantle values are from Sun & McDonough (1989). The shaded field shows the predominant trace-element range of Cenozoic basalts of SE China (Zou *et al.* 2000).

lower and upper crust (Fig. 7b). Mafic rocks from the Puchen dyke have relatively constant Y contents and Zr/Y ratios, suggesting minor involvement of crustal components. Nevertheless, all of these samples form a well-defined positive correlation between Nb and Yb, inconsistent with a crustal contamination trend (Fig. 7b), indicating these two elements were not significantly modified by crustal contamination.

In summary, rocks of the Lanpin, Xiamen and Damuchen dykes were strongly influenced by crustal contamination, and similar contamination has been recorded in Cretaceous mafic dykes elsewhere in SE China. For example, dykes from Jiangxi and Guangdong provinces have $^{87}Sr/^{86}Sr$ ratios up to 0.7140 (Li & McCulloch, 1998; Xie *et al.* 2006). On the other hand, samples from the Puchen, Maopin and Shaianjiao intrusions show only minor crustal contamination and can be used to constrain the evolution of their parental magmas. In addition, such elements as Nb and Yb were not significantly modified by crustal contamination in any of the Fujian intrusions and thus can be used to examine the nature of the mantle source region.

5.b. Nature of the mantle source and degree of partial melting

Zr and Y in primitive magmas are buffered by the mantle residuum (Pearce & Parkinson, 1993; Woodhead, Eggins & Gamble, 1993), and thus their concentrations are controlled mainly by variations in partial melting (McCulloch & Gamble, 1991; Stalder *et al.* 1998). More incompatible elements, such as Nb and Ta, are extremely sensitive to depletion/enrichment events because they enter the melt very efficiently (Pearce & Parkinson, 1993; Woodhead, Eggins &

https://doi.org/10.1017/S0016756807003834 Published online by Cambridge University Press

Table 3. Rb–Sr, Sm–Nd and Pb–Pb isotopic compositions for the mafic intrusions from the coastal area of Fujian Province, SE China

Sample no.	$^{87}Rb/^{86}Sr$	$^{87}Sr/^{86}Sr$	2δ	$(^{87}Sr/^{86}Sr)i$	$^{147}Sm/^{144}Nd$	$^{143}Nd/^{144}Nd$	2δ	$(^{143}Nd/^{144}Nd)i$	ε(Nd)	$^{208}Pb/^{204}Pb$	2δ	$^{207}Pb/^{204}Pb$	2δ	$^{206}Pb/^{204}Pb$	2δ
DK6	0.1267	0.707690	13	0.707565	0.1740	0.512348	10	0.512268	−5.5						
DK9	0.0924	0.706938	11	0.706847	0.1773	0.512692	10	0.512611	1.2						
DK11	0.1435	0.707481	14	0.707339	0.1829	0.512701	11	0.512617	1.4						
PC3	0.2723	0.707176	13	0.706753	0.1850	0.512880	9	0.512747	4.9						
PC4	0.0617	0.707403	11	0.707307	0.1729	0.512905	10	0.512780	5.5						
PC6	0.3596	0.707640	13	0.707082	0.1706	0.512871	9	0.512749	4.9						
DMC4	0.6502	0.708179	13	0.707446	0.1282	0.512431	13	0.512364	−3.3						
DMC7	0.3305	0.707843	13	0.707470	0.1275	0.512584	14	0.512517	−0.3						
DMC8	0.7134	0.708398	14	0.707592	0.1246	0.512443	11	0.512378	−3.1						
LP1	0.1923	0.706067	13	0.705845	0.1352	0.512502	10	0.512429	−2.0						
LP3	0.2329	0.705948	11	0.705678	0.1299	0.512771	10	0.512701	3.3						
TL5	0.1827	0.706249	13	0.705965	0.1349	0.512479	10	0.512382	−2.2						
TL7	0.2543	0.707055	14	0.706660	0.1315	0.512606	10	0.512511	0.3						
TL8	0.1520	0.706885	13	0.706649	0.1446	0.512592	9	0.512488	−0.2						
XM4	0.1132	0.706768	11	0.706637	0.1208	0.512725	10	0.512661	2.5						
XM6	0.2529	0.706728	13	0.706436	0.1144	0.512432	10	0.512371	−3.1						
XM7	0.1514	0.706848	14	0.706673	0.1204	0.512410	10	0.512345	−3.7						
SY14	0.1243	0.705540	13	0.705312	0.1591	0.512841	11	0.512706	4.6	38.641	19	15.633	07	18.410	08
SY18	0.1525	0.706454	11	0.706174	0.1418	0.512816	9	0.512695	4.4	38.448	30	15.504	12	18.424	14
SY19	0.2737	0.707168	13	0.706665	0.1521	0.512830	11	0.512700	4.5	38.692	14	15.623	06	18.522	07
SY20	0.2661	0.706465	10	0.705977	0.1578	0.512704	8	0.512570	1.9	38.731	10	15.649	03	18.503	04
XC2	0.6551	0.706678	13	0.705476	0.1504	0.512831	10	0.512703	4.5	38.445	13	15.563	05	18.352	06
XC4	0.7935	0.709208	11	0.707753	0.1484	0.512756	15	0.512630	3.1	38.774	12	15.664	05	18.500	05
XC5	0.1210	0.705130	13	0.704908	0.1370	0.512865	14	0.512748	5.4	38.217	15	15.479	06	18.260	06
XC7	0.3539	0.705331	13	0.704681	0.1552	0.512844	16	0.512712	4.7	38.690	14	15.639	06	18.483	06
XC8	0.0965	0.705189	13	0.705011	0.1506	0.512789	18	0.512661	3.7	38.730	08	15.670	02	18.479	02

Chondrite uniform reservoir (CHUR) values ($^{87}Rb/^{86}Sr = 0.0816$, $^{87}Sr/^{86}Sr = 0.7045$, $^{147}Sm/^{144}Nd = 0.1967$, $^{143}Nd/^{144}Nd = 0.512638$) are used for calculation. $\lambda_{Rb} = 1.41 \times 10^{-11}$ year^{-1}, $\lambda_{Sm} = 6.54 \times 10^{-12}$ year^{-1} (Lugmair & Marti, 1978). Both $(^{87}Sr/^{86}Sr)_i$ and ε_{Nd} were calculated by the mean K–Ar age 80 Ma for the Damuchen, Xiamen and Lanpin samples, 70 Ma for the Dancan samples, 110 Ma for the Tulin and Puchen samples and 130 Ma for the Maopin and Shaianjiao samples. K–Ar age data for calculation are from (J. H. Zhao, unpub. Honours thesis, Chinese Academy of Sciences, Institute of Geochemistry, 2004).

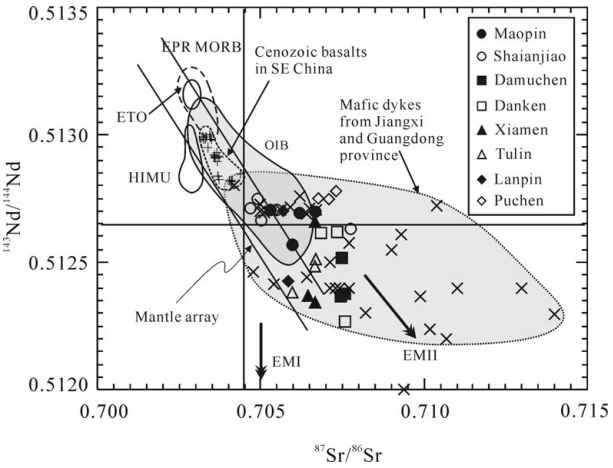

Figure 5. Initial $^{143}Nd/^{144}Nd$ v. $^{87}Sr/^{86}Sr$ ratios for the mafic rocks from the coastal area of Fujian province. The mafic rocks from Fujian province, together with these from Jiangxi (Xie *et al.* 2006) and Guangdong provinces (Li & McCulloch, 1998), form a trend extending roughly toward the EMII end-member. The approximate fields of DMM, EMI and EMII are from Zindler & Hart (1986). The fields for OIB, the East Taiwan Ophiolite (ETO), the East Pacific Rise MORB (Ho *et al.* 2003 and references therein) and Cenozoic basalts of SE China (Zou *et al.* 2000; Tu & Flower, 1991) are shown for comparison. Plus symbols (+) represent Cenozoic basalts of SE China, cross symbols (×) are Late Mesozoic mafic dykes in SE China from Xie *et al.* (2006) and Li & McCulloch (1998).

Gamble, 1993). Therefore, Nb, Zr, Y and Yb are all useful for estimating degrees of melting and mantle compositions (Münker, 2000).

Garnet has a high partition coefficient for Y ($D_{garnet/melt} = 4–11$) relative to Zr ($D_{garnet/melt} = 0.4–0.7$) (Jenner *et al.* 1993). Thus, the Zr and Y contents of primitive melts vary with the amount of garnet in the source region but the Zr/Y ratios of the melts correlate with Y contents. However, the partition coefficients of Zr and Y decrease from garnet peridotite ($D^{Zr}_{mantle/melt} = 0.04744$; $D^{Y}_{mantle/melt} = 0.26170$) to spinel–plagioclase lherzolite ($D^{Zr}_{mantle/melt} = 0.02735$; $D^{Y}_{mantle/melt} = 0.07468$). Accordingly, partial melting of a garnet peridotite mantle would produce a steeper trend in a Zr/Y v. Y diagram than melting of a spinel–plagioclase lherzolite mantle (Fig. 7a). Plots of Nb v. Yb (Fig. 7b) produce similar results. On a Zr/Y v. Y plot (Fig. 7a), type-A rocks from the Maopin and Shaianjiao mafic intrusions lie along the spinel lherzolite melting curve. Mafic rocks from the Puchen dyke (type P) have lower Y and Zr/Y ratios than those of the Maopin and Shaianjiao intrusions, but also plot along the spinel lherzolite melting curve. In the Nb v. Yb diagram, all of these rocks define a flat, positive trend, compatible with a spinel lherzolite source (Fig. 7b). Calculations suggest that the parental magmas of the Maopin and Shaianjiao intrusions were formed by 5–15 % partial melting of a spinel lherzolite. The parental magma of the Puchen dyke was formed from a similar source but experienced higher degrees of partial melting (Fig. 7a, b).

5.c. Enrichment of the lithospheric mantle

5.c.1. HFSE enrichment and EMII component in the source region

The samples from the Maopin and Shaianjiao intrusions were not significantly modified by crustal contamination, as discussed above, and therefore can be used to constrain the nature of their source. They are rich in Nb, ten times greater than primitive mantle melts with similar degrees of melting (Fig. 7b). Therefore, negative Nb anomalies on the primitive mantle-normalized trace element patterns indicate an enrichment of LILE rather than depletion of HFSE by subduction-related processes such as retention in the residual mantle or slab minerals as suggested by Münker (2000). The high Nb and Zr contents of the Maopin and Shaianjiao mafic rocks cannot be explained simply by melting of primitive mantle, suggesting enrichment of these elements in the mantle source.

On plots of Pb isotope compositions (Fig. 6a, b), samples from the Maopin and Shaianjiao intrusions, together with those from mafic dykes in Jiangxi province, fall to the left of the northern hemisphere reference line (NHRL). Compared with $^{206}Pb/^{204}Pb$ (18.26–18.522), the relatively large variations of $^{207}Pb/^{204}Pb$ (15.479–15.670) and $^{208}Pb/^{204}Pb$ (38.217–38.774) define a high-angle array away from the NHRL (Hart, 1984) that extends from Pacific MORB to EMII end-member (Fig. 6a, b). A generally positive correlation between $^{87}Sr/^{86}Sr$ and $^{206}Pb/^{204}Pb$ ratios and a negative correlation between $^{143}Nd/^{144}Nd$ and $^{206}Pb/^{204}Pb$ ratios also suggest that the mafic rocks have EMII-like components (Fig. 6c, d). It should be noted that four samples from the Jiangxi province have relative low $^{143}Nd/^{144}Nd$ and $^{206}Pb/^{204}Pb$ ratios, suggesting enriched mantle type I (EMI) may have been involved, although Xie *et al.* (2006) attributed this to mixing between EMII and depleted MORB mantle (DMM). Thus, the mafic rocks in SE China are not only enriched in HFSE, but also have EM-like components in their lithospheric mantle source.

5.c.2. OIB v. subducted sediment components in the source region

Two models are proposed to explain the nature of the mantle source (Fig. 6). The first model is mixing of a depleted asthenospheric mantle and an EMII-like lithospheric mantle source. The second model involves derivation of the melts from a depleted lithospheric mantle source which was contaminated by subduction components.

https://doi.org/10.1017/S0016756807003834 Published online by Cambridge University Press

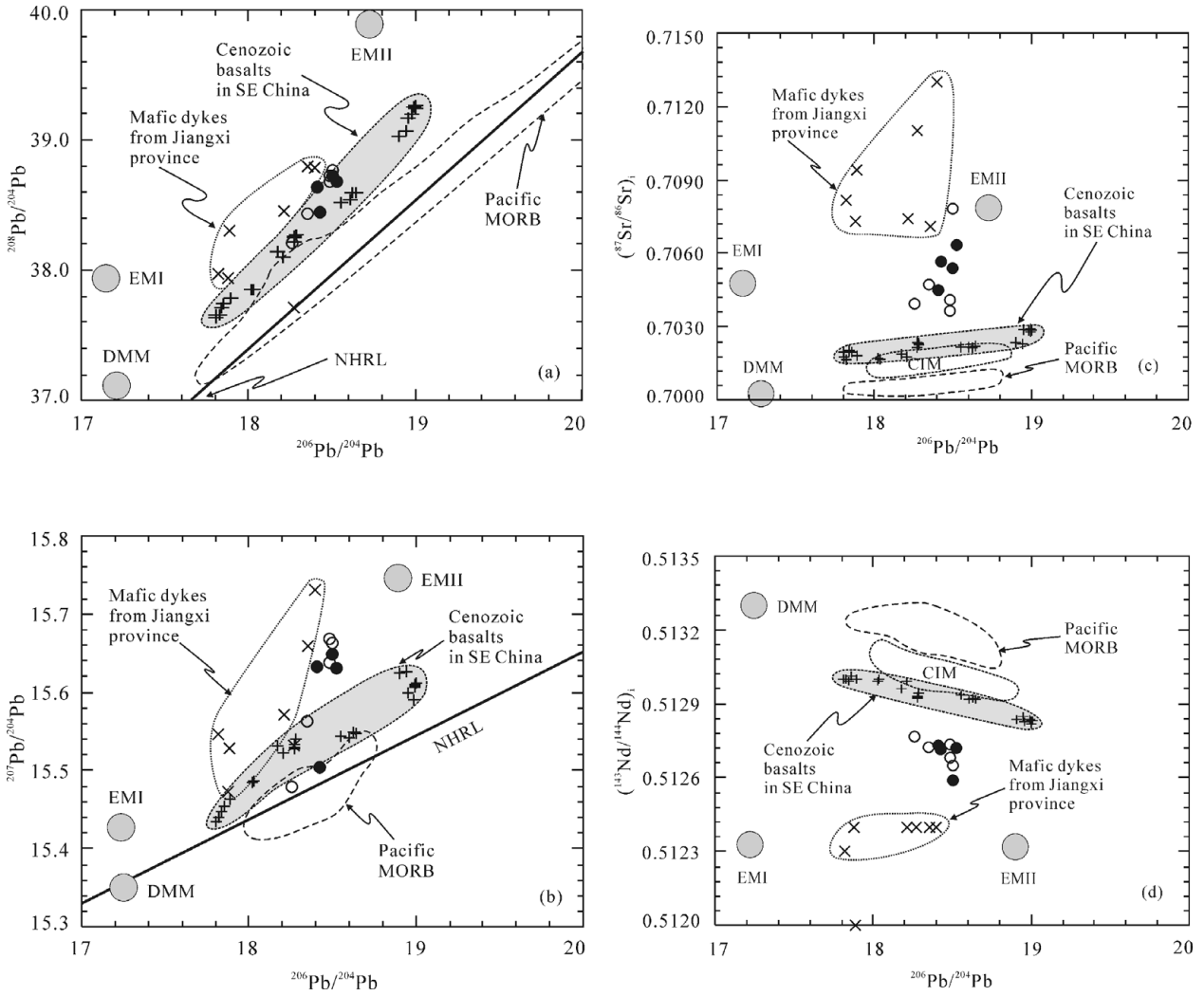

Figure 6. Plots of (a) $^{206}Pb/^{204}Pb$ v. $^{207}Pb/^{204}Pb$ ratios, (b) $^{206}Pb/^{204}Pb$ v. $^{208}Pb/^{204}Pb$ ratios, (c) $^{206}Pb/^{204}Pb$ v. initial $^{87}Sr/^{86}Sr$ ratios and (d) $^{143}Nd/^{144}Nd$ for the Maopin and Shaianjiao intrusions compared with Cenozoic basalts in SE China (Zou *et al.* 2000; Tu & Flower, 1991) and late Mesozoic mafic dykes from Jiangxi province (Xie *et al.* 2006). The samples with $^{206}Pb/^{204}Pb$ ratios less than 17.0 seem to show an EMI signature. NHRL is the Northern Hemisphere Reference Line (Hart, 1984). The approximate fields of DMM, EMI and EMII are from Zindler & Hart (1986). The fields for Pacific MORB and Central Indian MORB (CIM) are from Zou *et al.* (2000).

The relationship revealed in Figure 6 can be explained by mixing of a depleted asthenospheric mantle with an EMII-like lithosphere source. Depleted asthenospheric mantle beneath SE China has OIB-like geochemical characters as revealed by Cenozoic basalts (Qu, Taylor & Zhou, 1994; Chung *et al.* 1994; Zou *et al.* 2000; Ho *et al.* 2003), and such a mixing model has been proposed for some Mesozoic dykes in Jiangxi province (Xie *et al.* 2006). Although mixing of asthenospheric and lithospheric mantle would produce the good correlation between Pb and Sr isotopic ratios (Fig. 6) observed in the Fujian samples, it cannot explain their strong arc-like geochemical characteristics as shown on the primitive mantle normalized-trace element patterns (Fig. 4). The Fujian samples have trace element ratios distinctly different from OIB, N-MORB and Cenozoic basalts in SE China (Fig. 8, upper), and the negative correlation between Nb/Th and Nb/Yb in these rocks further rules out any contribution of asthenospheric components to their source (Fig. 8, lower).

Alternatively, the primary magmas may have originated from a lithospheric mantle that had been enriched in incompatible trace elements and modified isotopically by melts or fluids derived from a subducted slab (Hawkesworth *et al.* 1990; Mukasa, Fischer & Barr, 1996). Oceanic crust is composed of basaltic rocks covered by sediments. Melting of the MORB portion of the subducted slab requires unusually steep thermal gradients and is limited to young and relatively hot oceanic crust (Peacock, Rushmer & Thompson, 1994; Stern & Kilian, 1996). Subducted sediment therefore is a more likely source of Nb in this environment. Entrainment of subducted sediment into the mantle wedge occurs as melt rather than by bulk mixing (Nichols, Wyllie & Stern, 1994; Hawkesworth

https://doi.org/10.1017/S0016756807003834 Published online by Cambridge University Press

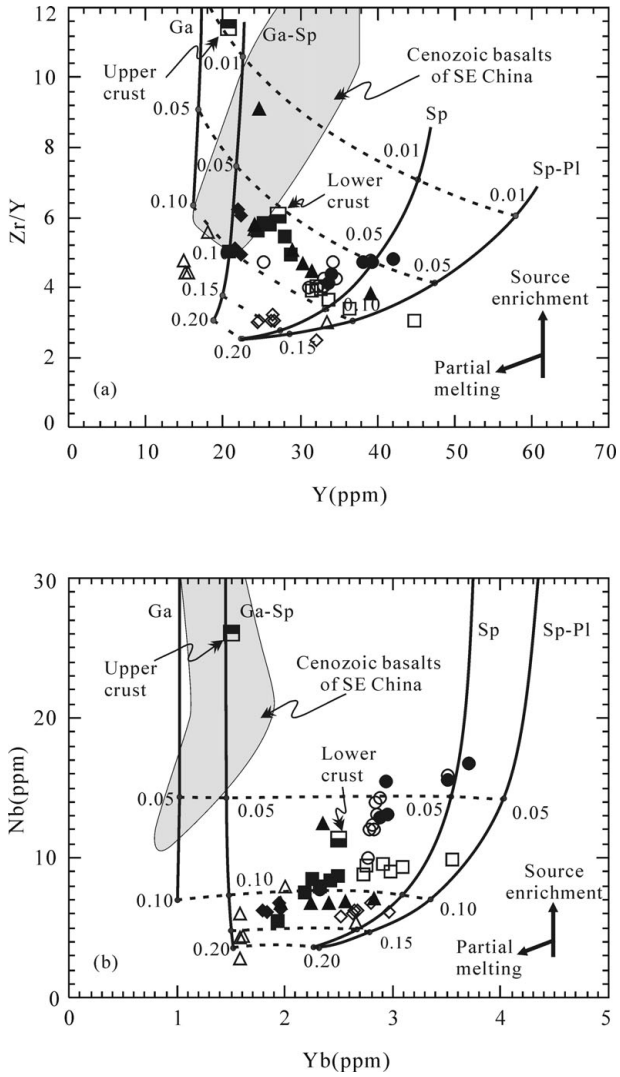

Figure 7. Plots of Y v. Zr/Y (a) and Nb v. Yb (b) for the mafic rocks from Fujian province in comparison with the calculated melting curves of garnet lherzolite (Ga), garnet-spinel lherzolite (Ga-Sp), spinel lherzolite (Sp) and spinel-plagioclase lherzolite (Sp-Pl). Labels along melting curves indicate degrees of partial melting (0.1 indicates 10 % melting). Starting compositions are assumed to be Pri-mantle (Sun & McDonough, 1989). Dashed lines are isograds of partial melting for different mantle sources. Partial melting partition coefficients (D values) are from Gorring & Kay (2001). Source and melt modes are given in Table 4, and the starting compositions are given in Table 5. The equation $C_L/C_o = (1-(1-PF/D)^{1/P})/F$ is used, where C_L is the element concentration in the melt. The data for Cenozoic basalts of SE China are also shown for comparison (Zou *et al.* 2000). Sample symbols are same as in Figure 2.

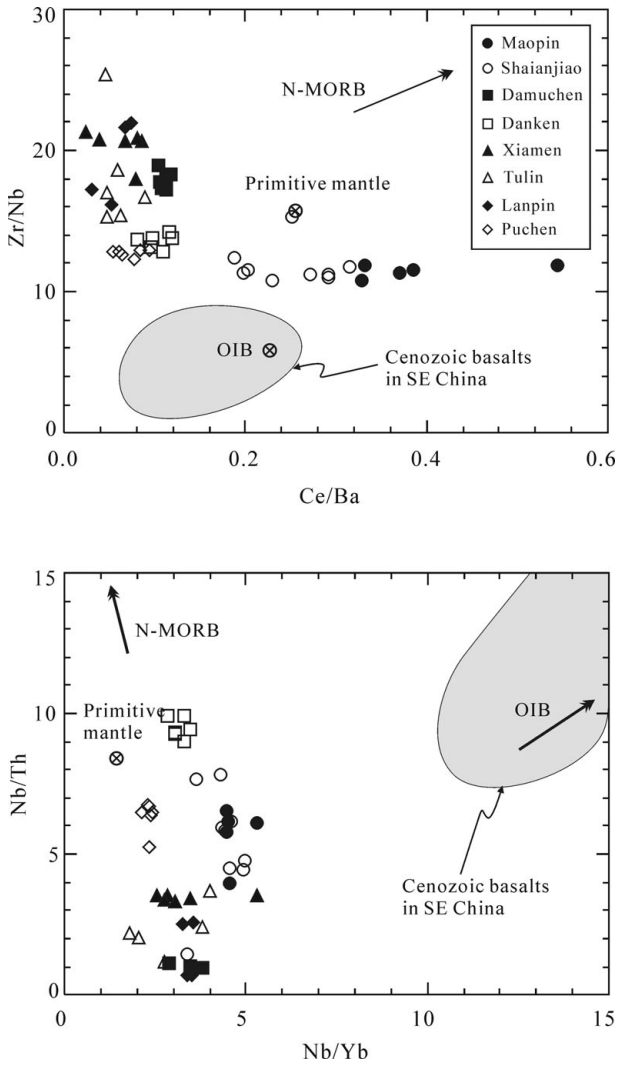

Figure 8. Plots of Zr/Nb v. Ce/Ba and Nb/Th v. Nb/Yb for the mafic rocks from the coastal area of Fujian province. Primitive mantle, OIB and N-MORB values are from Sun & McDonough (1989). Cenozoic basalts of SE China are from Zou *et al*. (2000).

et al. 1997). Calculations reveal that addition of less than 1 % subducted sediment-derived melt to the mantle wedge can explain the Nb compositions of the samples from Fujian province (Fig. 9). Samples from the Maopin and Shaianjiao intrusions experienced the highest source contamination, which is consistent with their position near the mixing line between the mantle wedge and Pacific sediment melts in Figure 10. Samples from the Puchen and Danken dykes approximately match the melting line of lherzolite mantle in Figure 9, suggesting no subducted slab melts were involved in their formation.

5.c.3. Enrichment by fluids from a subducted slab

In the $^{87}Sr/^{86}Sr$ v. Ba/Th diagram (Fig. 10), all of the Fujian samples fall to the right of the mixing line between the lithospheric mantle and sediment melts. The high Ba/Th ratios (29.8–1100) and their negative correlation with $^{87}Sr/^{86}Sr$ ratios imply the addition of another component to the mantle source of these rocks. Fluids derived from subducted slabs are the principal carriers of incompatible elements and promote metasomatism in the mantle wedge (Stolper & Newman, 1994; Johnson & Plank, 1999). Cervantes & Wallace (2003) demonstrated that fluxing of the wedge with an H_2O-rich component from the subducted slab is important in the formation of magmas rich in LILE

https://doi.org/10.1017/S0016756807003834 Published online by Cambridge University Press

Table 4. Source and melt modes used for melting calculations

Source modes						Melt modes						
Ol	Opx	Cpx	Pl	Sp	Ga	Ol	Opx	Cpx	Pl	Sp	Ga	Source
60	20	10	0	0	10	4	−19	105	0	0	10	Garnet peridotite[a]
55	22	15	0	2	6	−10	25	61	0	4	20	Ga-Sp lherzolite[b]
53	24	20	0	3	0	−30	40	82	0	8	0	Sp lherzolite[b]
55	24	15	5	1	0	−18	30	55	29	4	0	Sp-Pl lherzolite[b]

[a]Johnson (1998); [b]Gurenko & Chaussidon (1995).
Ol – olivine; Opx – orthopyroxene; Cpx – clinopyroxene; Pl – plagioclase; Sp – spinel; Ga – garnet.

Table 5. Mixing end-members used for model calculations

	Mantle wedge[1]	AOC fluid[2]	S[3]	S melt[4]	Crust[5]
Sr	21.1	180	325	2963	350
Nd	1.354	0.148	47.5	387	35
Pb	0.185	15	29.4	348	60
Nb	0.716	0.04	8.17	147	
Yb	0.493		4.99	1.77	
Ba	6.989	2210	1315	1769	
Th	0.085	1.69	6.55	131	
$^{87}Sr/^{86}Sr$	0.7025	0.7045	0.7074	0.7074	0.7300
$^{143}Nd/^{144}Nd$	0.51315	0.51315	0.51240	0.51240	0.51180
$^{207}Pb/^{204}Pb$	15.45	15.45	15.70	15.70	15.80
$^{206}Pb/^{204}Pb$	18.20	18.20	18.90	18.90	18.50

[1]Trace element concentrations are adopted from Sun & McDonough (1989). Isotopic composition is based on the data from White, Hofmann & Puchelt (1987) and Mahoney *et al.* (1994) at $^{143}Nd/^{144}Nd = 0.51315$.
[2]Altered Oceanic Crust (AOC) fluid after Dorendorf, Wiechert & Wörner (2000) and Ishizuka *et al.* (2003).
[3]Average sediment composition (S) after Plank & Langmuir (1998).
[4]Sediment melt (5%) (S melt) in equilibrium with sediment (40:40:20 by mass clinopyroxene:garnet:biotite), partition coefficients and accumulated fractional melting equation: $(C_L/C_0=1/F*[1-(1-F)^{1/D}])$ are from Münker (2000).
[5]Trace elements and isotopic compositions are estimated from Palaeo- to Meso-Proterozoic metamorphic rocks of South China (Yu *et al.* 2003). Pb, $^{207}Pb/^{204}Pb$ and $^{206}Pb/^{204}Pb$ are estimated from the Mesozoic granites in SE China (Zhang *et al.* 1994).

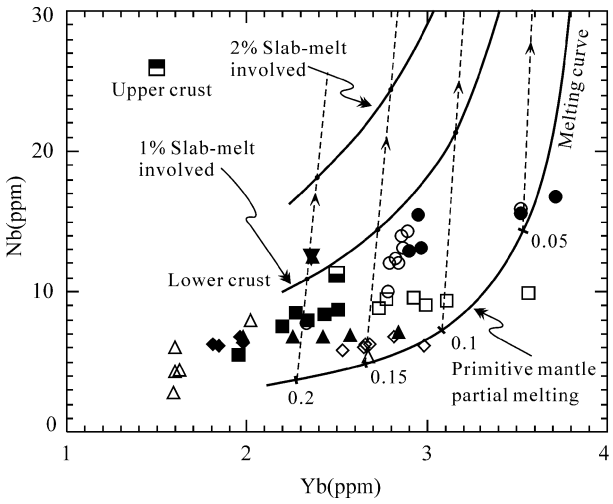

Figure 9. Plot of Nb v. Yb for the mafic rocks from Fujian province in comparison with the calculated mixing curves. Mixing end-members are partial melts of a spinel lherzolite mantle and Pacific sediment melts (5 % degree partial melting). Labels along curves indicate degree of partial melting. Dashed lines connect identical degrees of partial melting. Melting curve for spinel lherzolite is the same as in Figure 7, and sample symbols are the same as in Figure 2.

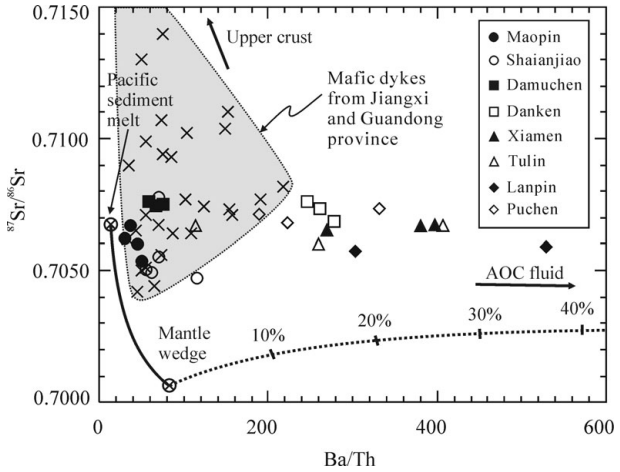

Figure 10. Plots of initial $^{87}Sr/^{86}Sr$ v. Ba/Th for the mafic rocks from the coastal area of Fujian province. Solid line is a mixing curve between the mantle wedge and the sediment melt. Dotted line is mixing curve between the mantle wedge and the slab-derived fluid. Labels along this line are percentage of fluids involved. Samples from the mafic dykes in the Jiangxi (Xie *et al.* 2006) and Guangdong provinces (Li & McCulloch, 1998) have high radiogenic $^{87}Sr/^{86}Sr$ ratios and low Ba/Th ratios, suggesting strong crustal contamination. Mixing end-members are listed in Table 5.

https://doi.org/10.1017/S0016756807003834 Published online by Cambridge University Press

and LREE relative to HFSE, producing a source with high LILE/HFSE ratios. The high Ba/Th ratios of the Fujian samples, especially those from the Xiamen and Tulin dykes, suggest that a large amount of slab-derived fluid was involved in their petrogenesis (Fig. 10).

Geochemically, the two different types of mafic rocks in Fujian province could have been produced by heterogeneous modification of the mantle source by subduction components. However, such a model cannot explain the high $^{87}Sr/^{86}Sr$ and $^{207}Pb/^{204}Pb$ ratios of the mafic rocks from the Maopin and Shaianjiao intrusions, which plot above the mixing line between DDM and average Pacific sediment melt, although the isotopic compositions of the Pacific sediments are assumed to have $^{87}Sr/^{86}Sr$ and $^{207}Pb/^{204}Pb$ ratios as high as 0.7150 and 15.80, respectively (Fig. 11a, b). In addition, samples from Jiangxi and Guangdong provinces have $^{87}Sr/^{86}Sr$ ratios as high as 0.714, suggesting that crustal contamination was widespread in eastern China. Thus, we propose that although crustal contamination played a major role in determining the geochemistry of these rocks, it did not significantly influence HFSE and HREE abundances, as discussed above. The isotopic variations of these rocks can be readily explained by a three-component mixing model: mantle wedge, crustal component and subducted sediment melt (Fig. 11). Less than 1 % source assimilation combined with 20 % crustal contamination can explain the chemical compositions in the Fujian mafic rocks. Some dykes, such as those from Jiangxi and Guangdong provinces, require more than 20 % crustal components to account for their composition (Fig. 11).

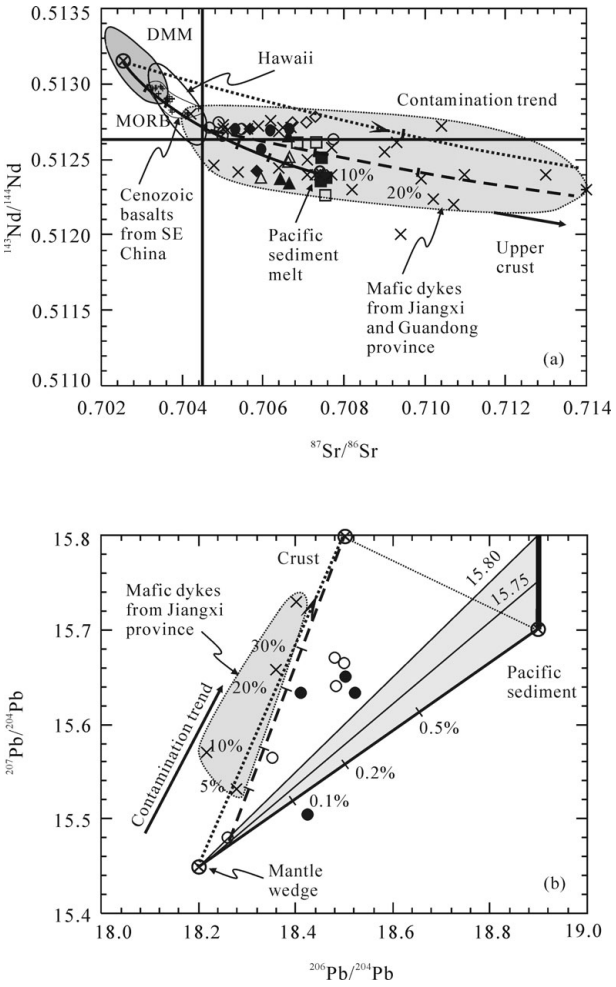

Figure 11. Plots of (a) $^{87}Sr/^{86}Sr$ v. $^{147}Nd/^{144}Nd$ ratios and (b) $^{206}Pb/^{204}Pb$-$^{207}Pb/^{204}Pb$ ratios for the rocks from the mafic dykes, SE China. Samples with $^{206}Pb/^{204}Pb$ less than 18 are not included due to their abnormal EMI features. Solid lines are mixing curves between the mantle wedge and the sediment melt. $^{207}Pb/^{204}Pb$ ratios for the subducted sediment are assumed to vary from 15.70 to 15.80 (Plank & Langmuir 1998). Shaded area represents source contamination field. Dotted lines with arrows are mixing lines between mantle wedge and continental crust components. Dashed line is calculated by mixing between sample XC5 and crustal components, labels along the curve are degrees of crustal contamination, suggesting that up to 20 % continental crust was involved in the magma petrogenesis. Mixing end-members used in the calculation are listed in Table 5. Sample symbols are same as in Figure 10.

5.d. Secular evolution of the lithospheric mantle beneath SE China

Geological and geophysical evidence indicates that at least 100 km of Archaean to Proterozoic lithospheric mantle has been removed beneath southeastern China since late Mesozoic times (Xu *et al.* 2000). This lithospheric thinning resulted from two separate episodes of chemical and mechanical modification.

Collision between the Palaeo-Pacific Plate and Eurasian Plate occurred in the Palaeozoic (Maruyama *et al.* 1997). Melts and fluids derived from the subducted Pacific slab were introduced into the lithospheric mantle during the Mesozoic, and the Proterozoic lithosphere was heterogeneously replaced by arc-like lithosphere (Zheng *et al.* 2004). Most mafic dykes in SE China show arc-like geochemical characteristics, suggesting widespread and extensive modification by slab materials (Li & McCulloch, 1998; Dong *et al.* 2006; Xie *et al.* 2006). The type-P rocks from the Puchen and Danken dykes show primitive mantle-like trace element patterns (Fig. 4b), suggesting that their source region may have been residual Proterozoic lithosphere.

During late Mesozoic times, subduction of the Palaeo-Pacific plate initiated continental extension, which led to upwelling of the asthenospheric mantle, producing voluminous felsic magmatism (Lapierre *et al.* 1997; Li, 2000) associated with mafic magmas (Li & McCulloch, 1998; Xie *et al.* 2006). This suggests that the Mesozoic lithosphere was hotter than the Palaeozoic lithosphere. The upwelling asthenosphere may have triggered melting of the previously enriched and highly modified lithosphere to produce the mafic dykes and plutons described in this paper. The occurrence of

https://doi.org/10.1017/S0016756807003834 Published online by Cambridge University Press

mafic dykes in Jiangxi, Fujian and Guandong provinces suggest that lithospheric extension was active and widespread in southeast China during late Mesozoic times.

Cenozoic basalts in SE China were mainly derived from asthenospheric mantle material (Flower *et al.* 1992; Liu, Masuda & Xie, 1994; Qu, Taylor & Zhou, 1994; Zou *et al.* 2000) and have OIB (Zou *et al.* 2000) and EMII-like signatures (Chung *et al.* 1995; Ho *et al.* 2003). Their formation was also related to asthenospheric upwelling and lithospheric extension (Yu *et al.* 2003), resulting in thermal and mechanical erosion. Sun & McDonough (1989) suggested that later intraplate melts may overprint or even erase arc-like geochemical signatures from lithospheric mantle that had been previously modified by subduction-related processes, but that EMII signatures would be preserved. The strong OIB character of the Cenozoic basalts in southeastern China suggests that the Mesozoic arc-like lithosphere in this region may have been consumed or completely modified. The EMII signatures of these basalts may have been derived from continental lithospheric mantle affected by Mesozoic subduction (Tu & Flower, 1991; Flower *et al.* 1992; Chung *et al.* 1994; Zhang *et al.* 1996).

6. Conclusions

(1) Most of the Mesozoic mafic plutons in SE China have arc-like geochemical features strongly indicating derivation from an EMII-like mantle source. Minor mafic dykes show primitive mantle-like trace element patterns and were probably derived from a mantle source unmodified by subduction.
(2) Parental magmas of the mafic rocks from the Fujian province are believed to have formed by about 5–15 % partial melting of a spinel lherzolite mantle source. The magmas for the type-A rocks were derived from subduction-modified lithospheric mantle, whereas the type-P rocks were derived from a mantle source unmodified by subduction. Both types of rocks experienced high degrees of crustal contamination.
(3) Proterozoic lithospheric mantle beneath SE China was heterogeneously modified by subduction components to become the Mesozoic arc-like lithospheric mantle. Subsequent upwelling of asthenospheric material in the Cenozoic completely erased the arc signatures of the mantle but preserved its EMII signature.

Acknowledgements. This work was jointly supported by the Knowledge-Innovation Program of the Chinese Academy of Sciences (KZCX3-SW-125) and Outstanding Young Researcher Awards from National Natural Sciences Foundation of China (40129001 and 49925309 to Hu and Zhou). We appreciate comments and constructive suggestions by journal editor Dr David Pyle and three anonymous reviewers.

References

CERVANTES, P. & WALLACE, P. J. 2003. Role of H_2O in subduction-zone magmatism: new insights from melt inclusions in high-Mg basalts from central Mexico. *Geology* **31**, 235–8.

CHEN, J. F. & JAHN, B. M. 1998. Crustal evolution of southeastern China: Nd and Sr isotopic evidence. *Tectonophysics* **284**, 101–33.

CHUNG, S. L., SUN, S. S., TU, K., CHEN, C. H. & LEE, C. Y. 1994. Late Cenozoic basaltic volcanism around the Taiwan Strait, SE China: product of lithosphere-asthenosphere interaction during continental extension. *Chemical Geology* **112**, 1–20.

CHUNG, S. L., JAHN, B. M., CHEN, S. J., LEE, T. & CHEN, C. H. 1995. Miocene basalts in northwestern Taiwan: Evidence for EM-type mantle sources in the continental lithosphere. *Geochimica et Cosmochimica Acta* **59**, 549–55.

DONG, C. W., ZHANG, D. R., XU, X. S., YEN, Q. & ZHU, G. O. 2006. SHRIMP U–Pb dating and lithogeochemistry of basic-intermediate dyke swarms from Jinjiang, Fujian Province. *Acta Petrologica Sinica* **22**, 1696–1702.

DONG, C. W., ZHOU, X. M., LI, H. M., REN, S. L. & ZHOU, X. H. 1997. Late Mesozoic crust-mantle interaction in southeastern Fijian – isotopic evidence from the Pingtan igneous complex. *Chinese Science Bulletin* **42**, 495–8.

DORENDORF, F., WIECHERT, U. & WÖRNER, G. 2000. Hydrated sub-arc mantle: a source for the Kluchevskoy volcano, Kamchatka/Russia. *Earth and Planetary Science Letters* **175**, 69–86.

FAN, W. M., ZHANG, H. F., BAKER, J., JARVIS, K. E., MASON, P. R. D. & MENZIES, M. A. 2000. On and off the North China Craton: where is the Archaean keel? *Journal of Petrology* **41**, 933–50.

FLOWER, M. F. J., ZHANG, M., CHEN, C. Y., TU, K. & XIE, G. H. 1992. Magmatism in the South China Basin 2. Post-spreading Quaternary basalts from Hainan Island, south China. *Chemical Geology* **97**, 65–87.

Geology and MINERAL RESOURCES BUREAU OF FUJIAN PROVINCE (GMRBF). 1985. *Regional geology of Fujian Province*. Beijing: Geological Publishing House (in Chinese).

GORRING, M. L. & KAY, S. M. 2001. Mantle processes and sources of Neogene slab window magmas from southern Patagonia, Argentina. *Journal of Petrology* **42**, 1067–94.

GURENKO, A. A. & CHAUSSIDON, M. 1995. Enriched and depleted primitive melts included in olivine from Icelandic tholeiites: Origin by continuous melting of a single mantle column. *Geochimica et Cosmochimica Acta* **59**, 2905–17.

HART, S. R. 1984 A large-scale isotope anomaly in the Southern Hemisphere mantle. *Nature* **309**, 753–7.

HAWKESWORTH, C. J., KEMPTON, P. D., ROGERS, N. W., ELLAN, R. M. & VAN CALSTEREN, P. W. 1990. Continental lithosphere, and shallow level enrichment processes in the Earth's mantle. *Earth and Planetary Science Letters* **96**, 256–68.

HAWKESWORTH, C. J., TURNER, S. P., MCDERMOTT, F., PEATE, D. W. & VAN CALSTEREN, P. W. 1997. U–Th isotopes in arc magmas: implications for element

transfer from the subducted crust. *Science* **276**, 551–5.

HO, K. S., CHEN, J. C., LO, C. H. & ZHAO, H. L. 2003. $^{40}Ar/^{39}Ar$ dating and geochemical characteristics of late Cenozoic basaltic rocks from the Zhejiang-Fijian region, SE China: eruption ages, magma evolution and petrogenesis. *Chemical Geology* **197**, 287–318.

ISHIZUKA, O., TAYLOR, R. N., MILTON, J. A. & NESBITT, R. W. 2003. Fluid-mantle interaction in an intra-oceanic arc: constraints from high-precision Pb isotopes. *Earth and Planetary Science Letters* **211**, 221–36.

JAHN, B. M., CHEN, P. Y. & YAN, T. P. 1976. Rb-Sr ages of granitic rocks in southeastern China and their tectonic significance. *Geological Society of America Bulletin* **86**, 763–76.

JENNER, G. A., FOLEY, S. F., JACKSON, S. E., GREEN, T. H., FRYER, B. J. & LONGERICH, H. P. 1993. Determination of partition coefficients for trace elements in high pressure-temperature experimental run products by laser ablation microprobe-inductively coupled plasmamass spectrometry (LAM-ICP-MS). *Geochimica et Cosmochimica Acta* **57**, 5099–130.

JIN, W. S. & SUN, D. Z. 1997. *Deep crustal structure of south China and its evolution*. Beijing Geological Publishing House (in Chinese).

JOHNSON, K. T. M. 1998. Experimental determination of partition coefficients for rare earth and high-field-strength elements between clinopyroxene, garnet, and basaltic melt at high pressure. *Contributions to Mineralogy and Petrology* **133**, 60–8.

JOHNSON, M. C. & PLANK, T. 1999. Dehydration and melting experiments constrain the fate of subducted sediments. *Geochemistry, Geophysics, Geosystems* **1**, 1999GC000014.

LAPIERRE, H., JAHN, B. M., CHARVET, J. & YU, Y. W. 1997. Mesozoic felsic arc magmatism and continental olivine tholeiites in Zhejiang Province and their relationship with the tectonic activity in southeastern China. *Tectonophysics* **274**, 321–38.

LI, H. M., DONG, C. W., XU, X. S. & ZHOU, X. M. 1995. Single zircon U–Pb chronological study on the gabbro from Quanzhou. *Chinese Science Bulletin* **40**, 158–60.

LI, X. H. 2000. Cretaceous magmatism and lithospheric extension in Southeast China. *Journal of Asian Earth Sciences* **18**, 293–305.

LI, X. H., LIU, D. Y., SUN, M., LI, W. X., LIANG, X. R. & LIU, Y. 2004. Precise Sm–Nd and U–Pb isotopic dating of the super-giant Shizhuyuan polymetallic deposit and its host gramite, Southeast China. *Geological Magazine* **141**, 225–31.

LI, X. H. & MCCULLOCH, M. T. 1998. Geochemical characteristics of Cretaceous mafic dykes from northern Guangdong, SE China: Age, origin, and tectonic significance. In *Mantle dynamics and plate interaction in East Asia* (eds M. F. J. Flower, S.-L. Chung, C.-H. Lo & T. Y. Lee), pp. 405–19. American Geophysical Union Geodynamics Series no. 27. Washington, DC.

LIU, C. Q., MASUDA, A. & XIE, G. H. 1994. Major and trace-element compositions of Cenozoic basalts in eastern China: Petrogenesis and mantle source. *Chemical Geology* **114**, 19–42.

LU, H. F., JIA, D., WANG, Z. H., GUO, L. Z., SHI, Y. S. & ZHANG, Q. L. 1994. Tectonic evolution of the Dongshan terrane, Fujian province, China. *Journal of South American Earth Sciences* **7**, 349–65.

LUGMAIR, G. W. & MARTI, K. 1978. Lunar initial $^{143}Nd/^{144}Nd$: differential evolution of the lunar crust and mantle. *Earth and Planetary Science Letters* **39**, 349–57.

MAHONEY, J. J., SINTON, J. M., KURZ, M. D., MCDOUGALL, J. D., SPENCER, K. J. & LUGMAIR, G. W. 1994. Isotope and trace element characteristics of a super-fast spreading ridge: East Pacific rise, 13–23°S. *Earth and Planetary Science Letters* **121**, 173–93.

MARUYAMA, S., ISOZAKI, Y., KIMURA, G. & TERABAYASHI, M. 1997. Paleogeographic maps of the Japanese islands: Plate tectonic synthesis from 750 Ma to the present. *The Island Arc* **6**, 121–42.

MCCULLOCH, M. T. & GAMBLE, J. A. 1991. Geochemical and geodynamical constraints on subduction zone magmatism. *Earth and Planetary Science Letters* **102**, 358–74.

MUKASA, S. B., FISCHER, G. M. & BARR, S. M. 1996. The character of the subcontinental mantle in Southeast Asia: isotopic and elemental compositions of extension-related Cenozoic basalts in Thailand. In *Earth processes: reading the isotopic code* (eds American Geophysical Union), pp. 233–52. AGU Monograph no. 95.

MÜNKER, C. 2000. The isotope and trace element budget of the Cambrian Devil River arc system, New Zealand: identification of four source components. *Journal of Petrology* **41**, 759–88.

NICHOLS, G. T., WYLLIE, P. J. & STERN, C. R. 1994. Subduction zone melting of pelagic sediments constrained by melting experiments. *Nature* **371**, 785–8.

PEARCE, J. A. & CANN, J. R. 1973. Tectonic setting of basic volcanic rocks determined using trace element analyses. *Earth and Planetary Science Letters* **19**, 290–300.

PEARCE, J. A. & PARKINSON, I. J. 1993. Trace element models for mantle melting: application to volcanic arc petrogenesis. In *Magmatic Processes and Plate Tectonics* (eds H. M. Prichard, T. Alabaster, N. B. W. Harris & C. R. Neary), pp. 373–403. Bath: Geological Society of London, Special Publication no. 76.

PEACOCK, S. M., RUSHMER, T. & THOMPSON, A. B. 1994. Partial melting of subducting oceanic crust. *Earth and Planetary Science Letters* **121**, 227–44.

PLANK, T. & LANGMUIR, C. H. 1998. The chemical composition of subducting sediment and its consequences for the crust and mantle. *Chemical Geology* **145**, 325–94.

QI, L., HU, J. & GREGOIRE, D. C. 2000. Determination of trace elements in granites by inductively coupled plasma mass spectrometry. *Talanta* **51**, 507–13.

QU, Q., TAYLOR, L. A. & ZHOU, X. M. 1994. Geochemistry and petrogenesis of three series of Cenozoic basalts from Southeastern China. *International Geological Review* **36**, 435–51.

STALDER, R., FOLEY, S. F., BREY, G. P. & HORN, I. 1998. Mineral-aqueous fluid partitioning of trace elements at 900–1200 °C and 3.0–5.7 GPa: New experimental data for garnet, clinopyroxene, and rutile, and implications for mantle metasomatism. *Geochimica et Cosmochimica Acta* **62**, 1781–1801.

STEIGER, R. H. & JÄGER, E. 1977. Subcommission on geochronology; convention on the use of decay constants in geochronology and cosmochronology. *Earth and Planetary Science Letters* **36**, 359–62.

STERN, C. R. & KILIAN, R. 1996. Role of the subducted slab, mantle wedge and continental crust in the generation of adakites from the Andean Austral Volcanic Zone.

Contributions to Mineralogy and Petrology **123**, 263–81.

STOLPER, E. & NEWMAN, S. 1994. The role of water in the petrogenesis of Mariana trough magmas. *Earth and Planetary Science Letters* **121**, 293–325.

SUN, S.-S. & MCDONOUGH, W. F. 1989. Chemical and isotopic systematics of oceanic basalts: implications for mantle composition and processes. In *Magmatism in the Ocean Basins* (eds A. D. Saunders & M. J. Norry), pp. 313–45. Geological Society of London, Special Publication no. 42.

TU, K. & FLOWER, M. F. J. 1991. Sr Nd and Pb isotopic compositions of Hainan basalts (South China): Implications for a subcontinental lithosphere Dupal source. *Geology* **19**, 567–9.

WANG, W. Y., SUEAO, S., TAKAHASHI, E., YURIMOTO, H. & GASPARIK, T. 2000. Enrichment processes at the base of the Archean lithospheric mantle: observations from trace element characteristics of pyropic garnet inclusions in diamonds. *Contributions to Mineralogy and Petrology* **139**, 720–33.

WANG, Z. H. 2002. The origin of the Cretaceous gabbros in the Fujian coastal region of SE China: implications for deformation-accompanied magmatism. *Contributions to Mineralogy and Petrology* **144**, 230–40.

WHALEN, J. B., SYME, E. C. & STERN, R. A. 1999. Geochemical and Nd isotopic evolution of Paleoproterozoic arc-type granitoid magmatism in the Flin Flon Belt, Trans-Hudson orogen, Canada. *Canadian Journal of Earth Sciences* **36**, 227–50.

WHITE, W. M., HOFMANN, A. W. & PUCHELT, H. 1987. Isotope geochemistry of Pacific mid-ocean ridge basalt. *Journal of Geophysical Research* **92**, 4881–93.

WOODHEAD, J. D., EGGINS, S. & GAMBLE, J. 1993. High field strength and transition element systematics in island arc and back-arc basin basalts: evidence for a multiphase melts extraction and a depleted mantle wedge. *Earth and Planetary Science Letters* **144**, 491–504.

XIE, G. Q., HU, R. Z., FRANCO, P., LI, R. L., CAO, J. J., JIANG, G. H. & ZHAO, J. H. 2006. K–Ar Dating, Geochemical, and Sr–Nd–Pb Isotopic Systematics of Late Mesozoic Mafic Dikes, Southern Jiangxi Province, Southeast China: Petrogenesis and Tectonic Implications. *International Geological Review* **48**, 1023–51.

XU, X. S., O'REILLY, S. Y., GRIFFIN, W. L. & ZHOU, X.,2000. Genesis of young lithospheric mantle in Southeastern China: an LAM-ICPMS trace element study. *Journal of Petrology* **41**, 111–48.

Yu, J. H., Xu, X. S., O'REILLY, S. Y., GRIFFIN, W. L. & ZHANG, M. 2003. Granulite xenoliths from Cenozoic Basalts in SE China provide geochemical fingerprints to distinguish lower crust terranes from the North and South China tectonic blocks. *Lithos* **67**, 77–102.

ZHANG, H. F. & SUN, M. 2002. Geochemistry of Mesozoic basalts and mafic dykes, Southeastern North China Craton, and tectonic implications. *International Geological Review* **44**, 370–82.

ZHANG, H. F., SUN, M., ZHOU, X. H., ZHOU, M. F., FAN, W. M. & ZHENG, J. P. 2003. Secular evolution of the lithosphere beneath the eastern North China Craton: Evidence from Mesozoic basalts and high-Mg andesites. *Geochimica et Cosmochimica Acta* **67**, 4373–87.

ZHANG, L. G., WANG, K. F., CHEN, Z. S., LIU, J. X., YU, G. X., WU, K. L. & LAN, J. Y. 1994. On 'Cathaysia'-Evidence from lead isotope study. *Geological Review* **40**, 200–8 (in Chinese).

ZHANG, M., TU, K., XIE, G. H. & FLOWER, M. F. J. 1996. Subduction-modified subcontinental mantel in South China: trace element and isotope evidence in basalts from Hainan Island. *Chinese Journal of Geochemistry* **15**, 1–19.

ZHAO, J. H., HU, R. Z. & LIU, S. 2004. Geochemistry, petrogenesis, and tectonic significance of Mesozoic mafic dykes, Fujian Province, Southeastern China. *International Geological Review* **46**, 542–57.

ZHENG, J. P., O'REILLY, S. Y., GRIFFIN, W. L., ZHANG, M., LU, F. X. & LIU, G. L. 2004. Nature and evolution of Mesozoic–Cenozoic lithospheric mantle beneath the Cathaysia block, SE China. *Lithos* **74**, 41–65.

ZHOU, M.-F., ZHAO, J. H., QI, L., SU, W. C. & HU, R. Z. 2006. Zircon U–Pb geochronology and elemental and Sr–Nd isotope geochemistry of Permian mafic rocks in the Funing area, SW China. *Contributions to Mineralogy and Petrology* **151**, 1–19.

ZINDLER, A. & HART, S. R. 1986. Chemical geodynamics. *Annual Review of Earth and Planetary Sciences* **14**, 493–571.

ZOU, H. B., ZINDLER, A., XU, X. S. & QU, Q. 2000. Major, trace element, and Nd, Sr and Pb isotope studies of Cenozoic basalts in SE China, mantle sources, regional variations, and tectonic significance. *Chemical Geology* **171**, 33–47.